NTNU – Trondheim
Norwegian University of
Science and Technology

Application of Modular Multilevel Converter for Interfacing Grid-Connected Photovoltaic Conversion Plants

Eirik Grønvold Eggum

Master of Energy and Environmental Engineering
Submission date: June 2015
Supervisor: Lars Einar Norum, ELKRAFT

Norwegian University of Science and Technology
Department of Electric Power Engineering

Problem Description

The aim of this thesis is to investigate the feasibility of using Modular Multilevel Converter as interface between large-scale pv farms and the grid.

Abstract

This thesis investigates the applicability of the Modular Multilevel Converter (MMC) for interfacing grid connected photovoltaic conversion plants.

A detailed three-phase 9-level simulation model is implemented in Simulink. Two control objectives are identified as distinctive for the MMC: Capacitor voltage balancing and suppression of circulating currents, both of which are included in the model. The MMC is controlled by a modified Level-Shifted Pulse Width Modulator. The model is verified by comparing its behaviour to that of the mathematical model of the MMC.

The nature of photovoltaic power generation makes Maximum Power Point Tracking (MPPT) important to maximize the power yield from a pv module. All the pv modules connected to the same MPP tracker should have the same operating conditions. For large-scale pv farms this is only feasible with multiple MPP trackers.

Two pv inverter configurations are identified as suitable for grid connection of large-scale pv farms using the MMC: Cascaded dc-dc converters and multi-string inverter. With the former, the three phase legs share the same dc link voltage. With a multi-string topology, each submodule is fed by a separate pv string. Thus, power imbalance between the submodules are inevitable. This can be remedied by power imbalance compensation.

For grid side control Synchronous Reference Frame Control (SRFC) and Model Predictive Control (MPC) is considered. MPC has the advantage of handling non-linear constraints on both states and variables. In addition it is reported to perform better than SRFC during dynamic conditions, which are likely to occur with power generation from pv modules.

SRFC is implemented in the MMC simulation model. It synchronizes with the grid and delivers power at unity power factor.

Sammendrag

Denne hovedoppgaven undersøker muligheten for benytte en flernivå frekvens-omformer (MMC) for nettilkobling av solcelleanlegg.

En tre-fase simuleringsmodell er implementert i Simulink. To kontrollmål er identifisert som særegne for MMC: Balansering av kondensatorerspenninger og eliminering av sirkulerende strømmer. Begge disse kontrollmålene er implementert i modellen. Simuleringsmodellen er styrt av en modifisert nivå-skiftet puls bredde modulator. Modellen er verifisert ved å sammenligne dens oppførsel med den matematiske modellen av MMC.

Ved kraftproduksjon fra solceller er MPPT strengt nødvendig for å maksimere effektutbyttet. Alle solceller koblet til samme MPPT burde operere under samme sol- og temperaturforhold. For storskala solcelleanlegg er dette kun mulig med flere MPPTer.

To omformertopologier er identifisert som passende for nettilkobling av storskala solcelleanlegg: Topologi basert på kaskadekoblede dc-dc omformere og multi-streng omformer. For førstnevnte deler de tre fasene samme dc bru. Med multi-streng topologi er hver submodul matet av en separat pv-streng. Dette betyr at hver submodul vil motta forskjellig effekt. Dette må kompanseres for.

For styring av MMCen har dq-kontroll og modell predikativ kontroll (MPC) blitt vurdert. Fordelen med MPC er at den takler ikke-lineære begrensninger på både tilstander og variabler. I tillegg presterer den bedre enn dq-kontroll under dynamiske forhold, noe som vil inntre ofte ved kraftproduksjon fra solceller.

Dq-kontroll er implementert i simuleringsmodellen. MMCen synkroniseres med nettet og leverer effekt med $\cos(\phi) = 1$

Preface

I am thankful to my supervisor, Professor Lars Norum, who has given me the opportunity to work with this very interesting topic, and has provided valuable feedback during the semester. Secondly, I am in deep gratitude to Dr. Amin Hajizadeh, whose commitment to helping and joyous spirit has been a true inspiration.

Without these two, this thesis would not have been possible.

Eirik Eggum
June 2015

Table of Contents

List of Figures

Part I

Introduction

Chapter 1

Introduction

1.1 Background

Due to the possibility of providing energy with less dependence on the fossil fuels, renewable energy sources, in particular solar photovoltaic (PV) conversion have gained increased acceptance and growth in recent times. Significant advantages of pv panels include clean and reliable energy production and suitability for distributed generation. In addition the prices for photovoltaic modules is drastically decreasing. In fact, it is expected that the PV global installed capacity can reach up to 3000 GW, approximately 11% of the global electricity production by 2050. Considerable research attention is currently on-going for deploying the multilevel topologies for photovoltaic power conversion [1] [2] [3]. Multilevel inverters offer low total harmonic distortion, switching frequency, dv/dt and device voltage stress [4]. Valuable improvements can be made on the side of inverters for pv systems, as these account for approximately 15.25 % of the system costs [5]. Among the multilevel topologies, the Modular Multilevel Converter (MMC) is one of the most promising, and has received considerable attention in academia and industry lately. The modular structure, low device ratings, easy scalability and the possibility of using redundant cells for fault tolerant applications are some of the key features of this converter [6].

1.2 Scope of Work

This study focuses on the applicability of Modular Multilevel Converter for grid connection of pv systems.

The work is carried out as a literature review supported by computer simulations. In the literature review, analytical models for the MMC and a pv module are studied. In addition, the possible system configurations, function blocks and requirements for pv inverters are investigated.

Based on the theoretical model of the MMC, a detailed 9-level simulation model is implemented in Matlab/Simulink using the SimPowerSystems toolbox. As the MMC is the main focus of the thesis, the pv system is modelled using a block from the Simulink library.

Based on the properties of pv generation, the MMC and general pv inverter requirements, an MMC based pv inverter with full control system is proposed.

Several MMC submodule topologies are reported in literature. To limit the scope of the thesis, only the half bridge submodule topology is considered.

1.3 Report Outline

The thesis is organized in three parts: *Introduction*, *Method* and *Results, Discussion and Concluding Remarks*.

Part 1 provides an introduction to the topic and the necessary background theory. The topology, principle operation and primary control objectives of the Modular Multilevel Converter is presented in chapter 2. Chapter 3 presents an introduction to photovoltaics. Chapter 4 presents information on pv inverter families, function blocks, requirements and future prospects for pv inverters.

Part 2 is about modelling. Chapter 5 presents a mathematical model and a simulation model of the MMC. Implemented in the simulation model is capacitor voltage balancing and circulating current suppression. In chapter 6, a mathematical model of a pv array is presented. In addition, the importance of Maximum Power Point Tracking for maximizing the power yield from a pv farm is treated. Chapter 7 presents possible pv inverter topologies based on the properties of the MMC and photovoltaic power generation, as well as the general requirements discussed in chapter 4

Part 3 provides the most important results from the simulation, discussion of the main findings and concluding remarks.

Chapter 2

Principles of the Modular Multilevel Converter

Some of the information in this section is based on the project thesis presented by the author in fall of 2014. It is reproduced here for completeness

Since it was introduced in 2001 [7], the Modular Multilevel Converter has quickly reached maturity for hvdc applications. Now attention in industry and academia is turned to other areas of application. This chapter introduces the MMC. Main aspects are the converter topology, principle operation and main control objectives.

2.1 Topology

Converter The topology of a three phase MMC is shown in figure 2.1. It has one converter leg per phase, each consisting of an upper and a lower arm. The arms are comprised of n identical submodules connected in series and an inductor. The inductor is added to suppress high frequency components in the arm current, as well providing protection against short circuit currents in case of short circuiting on the dc side [6]. In high voltage applications n may be as high as several hundreds [8]. Resistors can be added to model the power losses related to switching of the IGBTs and conduction losses. In this thesis the resistors are modelled in series, but they can be added in parallel with the MMC legs as proposed in [9] as well.

Submodules The most common submodule topology, the half bridge, is shown in figure 2.2. It consists of two IGBTs with anti parallel diodes and a floating capacitor. Several other submodule topologies are possible, eg. H-bridge, unidirectional cell, multilevel NPC cell and multilevel flying capacitor cell [11]. In an effort to limit the scope of the thesis, only the half-bridge submodule has been considered. The main advantage of the half bridge submodule topology is its simplicity and low component count. With the capacitors

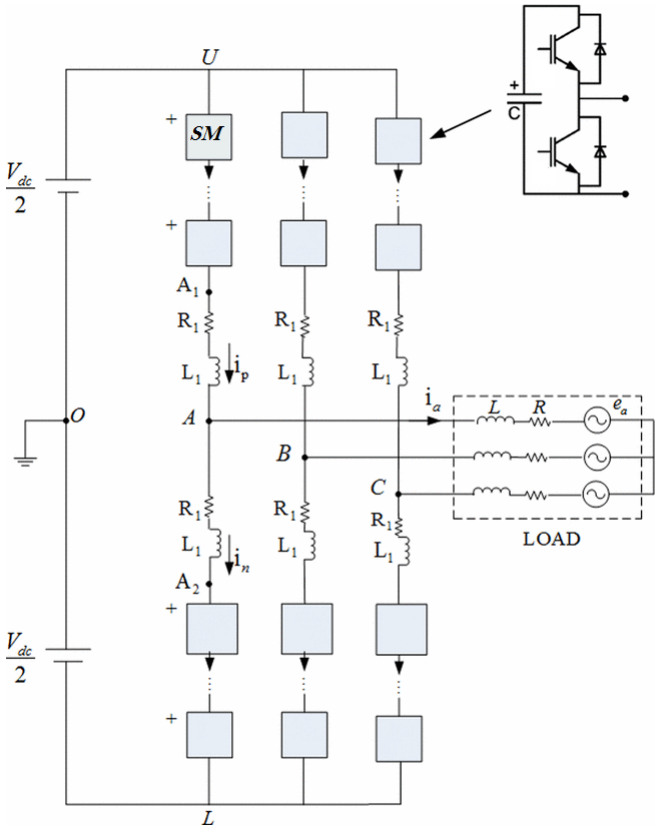

Figure 2.1: Topology of a three phase MMC [10]

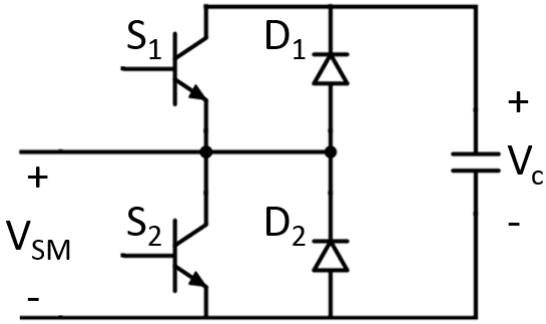

Figure 2.2: Submodule topology

included in the submodules the total capacitance of the MMC is generally larger than that of topologies with a single capacitance. However, the advantage of separating the capacitative elements is that the converter has no central components such as the large dc link capacitor of conventional voltage source inverters. Omitting the dc link capacitor is advantageous because it eases the protection of the converter against mechanical destruction in the case of short circuits or insulation failures [7]. The dc link capacitor can be omitted because the currents in the converter arms are not chopped, but rather flow continuously. This is another distinct feature of the MMC [12]

2.2 Principle Operation

Depending on the gating signal to the switches, the half bridge submodule terminal voltage, V_{SM}, is either zero or equal to the capacitor voltage, V_c. Ideally, V_c should be equal to V_{dc}/n, where V_{dc} is the dc link voltage. Since each submodule can be controlled separately, each converter arm is in principle a discrete leveled (0, $V_d/2$, ..., $nV_d/2$) controllable voltage source. Figure 2.4 shows the possible switching states of a single submodule during normal operation. The two switches are complementary during normal operation, meaning that when one is ON, the other is OFF. When S1 is ON and S2 is OFF, the submodule terminal voltage is equal to the capacitor voltage, and the capacitor is charging or discharging depending on the direction of the current through the submodule. When in this mode, the submodule is referred to as *inserted*. In the opposite case, when S1 is OFF and S2 is ON, the capacitor is *bypassed* and the submodule terminal voltage is zero. The capacitor voltage of a cell remains constant for as long as it is bypassed. During start up, both switches of a submodule can be OFF to charge the capacitors to their desired initial value. Both switches will never be ON at the same time, as this will cause the floating capacitor to short circuit [7]. For the MMC to operate properly, the capacitor voltage of every cell must be carefully kept close to the ideal value of V_{dc}/n. At any given moment a total of n submodules are inserted in each leg such that the total voltage across a leg ideally equals the voltage of the dc link.

$$n = n_{up} + n_{low} \tag{2.1}$$

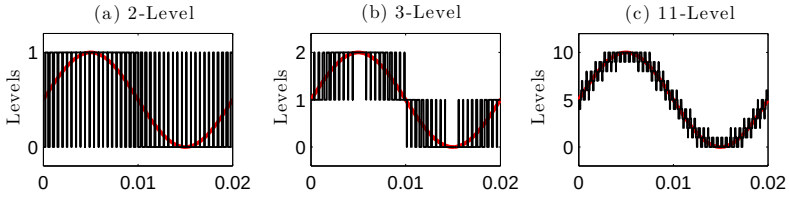

Figure 2.3: Multilevel waveforms, higher number of available voltage levels gives a smoother curve. (a) 2-Level. (b) 3-Level. (c) 11-Level

where n_{up} and n_{low} are the number of submodules inserted in the upper and lower arm respectively. Thus for a given voltage level increasing n will give a smoother output curve, as shown in figure 2.3, at the cost of increased component count.

Output waveforms Figure 2.5 displays the ideal waveforms for one phase of the MMC, ie. the output waveforms when $n \to \infty$. The insertion and bypassing of submodules is done so that the upper and lower arm voltages are in counter phase. The arm voltages can be mathematically expressed as [13]:

$$v_{UA_1} = \left[\frac{1}{2} + m' \sin(\omega t)\right] V_{dc} \tag{2.2a}$$

$$v_{A_2U} = \left[\frac{1}{2} - m' \sin(\omega t)\right] V_{dc} \tag{2.2b}$$

where m' is the sinusoidal modulation index ($0 \leq m' \leq 0.5$). Neglecting the voltage drop across the arm inductor, the phase-to-neutral output voltage for the MMC becomes an ideal sine wave with zero offset and amplitude mV_{dc}.:

$$v_{A0} = v_{A_1U} + v_{U0} = m' \sin(\omega t) V_{dc} \tag{2.3}$$

2.3 Control Objectives

The increased complexity of the topology places high demands on the control strategy. There are primarily four control objectives that must be met in order for the MMC to operate properly [12]:

1. *Submodule Capacitor Voltage Control:*
   As mentioned in section 2.2 the capacitors of the submodules charge or discharge depending on the switching states and the direction of the arm currents. A proper control scheme must regulate the stored energy in the capacitors such that the voltage of each submodule is approximately V_{dc}/n. The acceptable deviation from this value is dependent upon the application, but should generally be as small as possible. In addition to being balanced within each arm, the stored energy of the capacitors

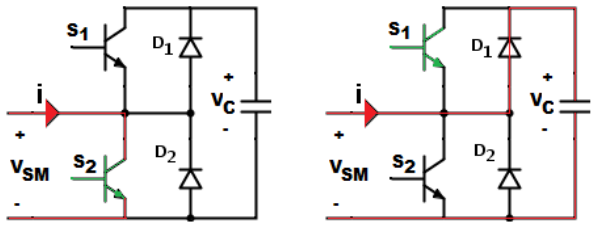

(a) Bypassed **(b)** Inserted, charging

(c) Inserted, discharging **(d)** Bypassed

Figure 2.4: Possible switching states during normal operation for the half bridge submodule

must be balanced within phase and among the phases. In steady state the following power balance must exist:

$$\underbrace{\frac{C_{eq}}{2}\frac{d}{dt}v_{cavg}^2}_{\substack{\text{Variation of energy}\\ \text{stored in capacitors}}} = \underbrace{v_{in}i_{in}}_{\text{Input power}} - \underbrace{v_{out}i_{out}}_{\text{Output power}} - P_{Loss} \tag{2.4}$$

where C_{eq} is the equivalent capacitance of the entire MMC. Balance between submodules of an arm can be achieved by employing a sorting algorithm [14], which will be explained in section 5.3.

2. *Current control:*
Voltage differences between the upper and lower arm of a leg and capacitor voltage ripples will give rise to circulating currents within the MMC. These currents will not affect the ac or dc side of the converter, but will increase the current magnitude flowing through each submodule. Consequently, they cause increased losses and will require higher rated components in the converter. In addition, a high circulating current will increase the voltage ripples in the submodules. Thus, the circulating current should be minimized. Several techniques have been proposed to minimize the circulating current. The simplest way is by means of increasing the arm inductance L_1, as proposed in [15]. This however, is not an ideal solution since it leads to increased losses, decreasing the overall performance of the MMC. Other proposals involve separately altering the modulation index of each arm [16], and more advanced controllers such as the repetitive controller proposed in [17].

3. *Active and Reactive Power Control*
   As for any VSC, a well designed control system for the MMC should keep the controlled variables close to the desired reference. A conventional dq-controller, as will be introduced in section 7.1.1, is applicable for this purpose for the MMC. Another possibility is Model Predictive control, which is introduced in section 7.1.2.

4. *DC link voltage control*
   The dc voltage of conventional VSCs are determined by the dc link capacitor voltage, which is omitted in the MMC. If maximum power is to be extracted from the pv system on the source side, the dc bridge voltage is determined by the operating conditions of the pv modules.

2.4 Pulse Width Modulation

Pulse Width Modulation (PWM) is the most common control method for the submodules of the MMC. Space vector modulation is also applicable [18]. However, due to the large number of possible vector combinations, PWM is chosen in this thesis. Several PWM strategies for controlling MMC have been proposed in literature. *Multicarrer* techniques are most common. In these methods multiple high frequency triangular carriers are compared to a reference signal. The two most common are phase-shifted and level-shifted PWM. The literature is inconclusive in which of these is the preferred. In this thesis only level-shifted PWM is considered. Each carrier is assigned to one or more submodules and compared to the reference signal. If the magnitude of the reference signal is greater than the magnitude of the carrier, the submodule is inserted, otherwise it is bypassed. The principle is demonstrated in figure 2.6. A significant drawback with multicarrier PWM is the need to synchronize the carriers. Failure to achieve synchronization may cause delay between devices that are supposed to turn on or off at the same time [13]. This can cause short circuiting of the submodule capacitors.

Since any real MMC will have a limited number of submodules, the waveforms shown in figure 2.5 are unattainable as output voltage. They can however be used as reference signal for the PWM. The amplitude of the reference signal is referred to as the modulation index, m. Increasing m above unity is called overmodulation. This increases the dc bus utilization, but causes distortion on the ac side output waveforms. Instead, it is possible to include a third harmonic component in the reference to increase the dc bus utilization [14]. This is explained in section 5.4.

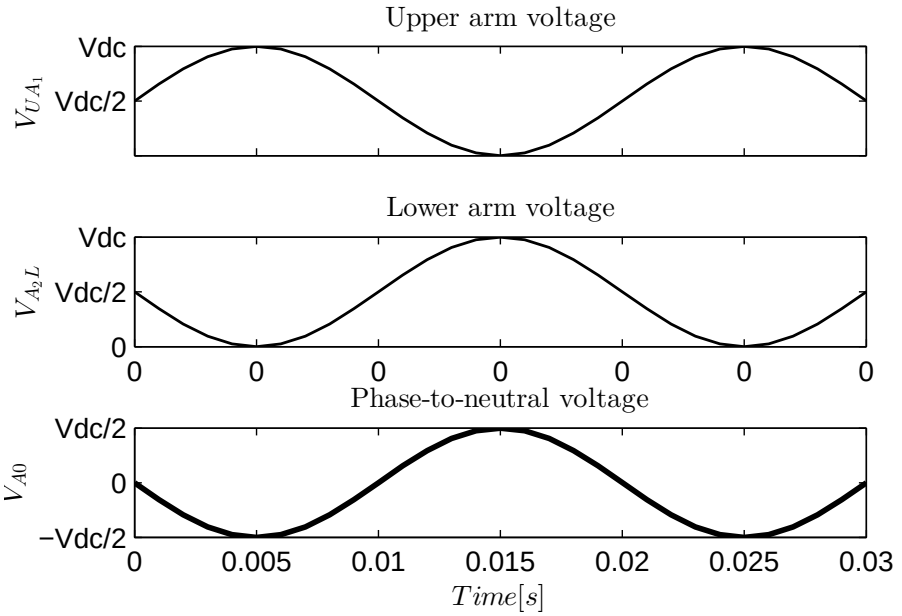

Figure 2.5: Ideal output waveforms for one phase of the converter.

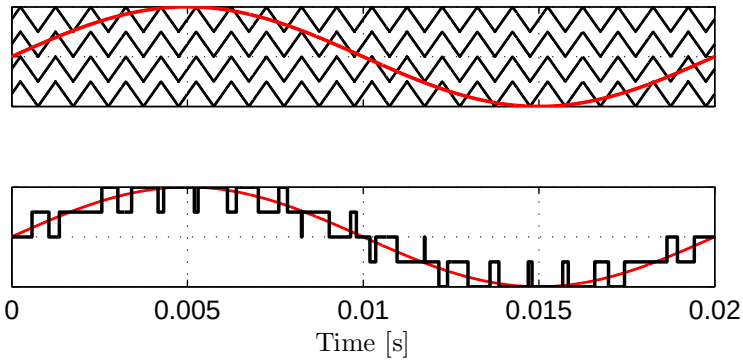

Figure 2.6: Demonstration of level shifted PWM. Upper: carriers, lower: resulting waveform.

Chapter 3

Principles of Photovoltaics

This section presents a brief introduction to photovoltaics. The ideal model for a pv cell is introduced, as well as some important pv parameters. The physical mechanisms and inner working of the PV-cell are beyond the scope of this thesis, and will not be explained. Photovoltaic cells are designed to take advantage of the photovoltaic effect, ie. the creation of voltage or electric current in materials upon exposure to light. As of today monocrystaline, polycrystaline and amorphous silicon are the most commonly used materials for manufacturing pv cells [19]. Since the power from a single cell is small, numerous cells are connected in series and parallel to form a PV array with higher power. Connecting cells in series provides greater output voltage, whilst cells connected in parallel increase the current.

Figure 3.1 shows the current-voltage (IV) curve of an ideal pv module for a given set of operating conditions. The curve is highly non-linear and sensitive to external factors such as temperature and irradiance.

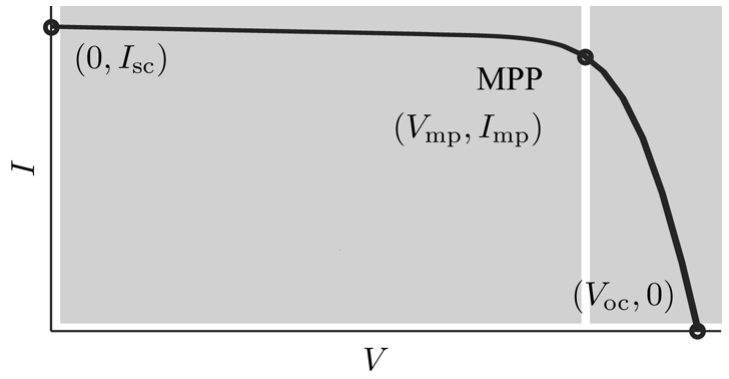

Figure 3.1: Characteristic IV curve of a practical pv device with three remarkable points [20].

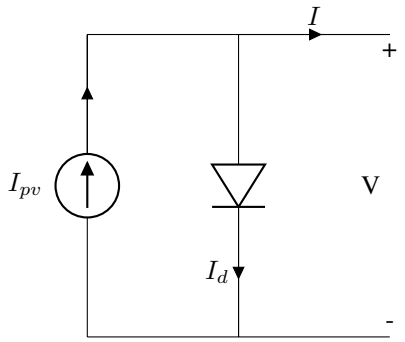

Figure 3.2: Ideal pv cell.

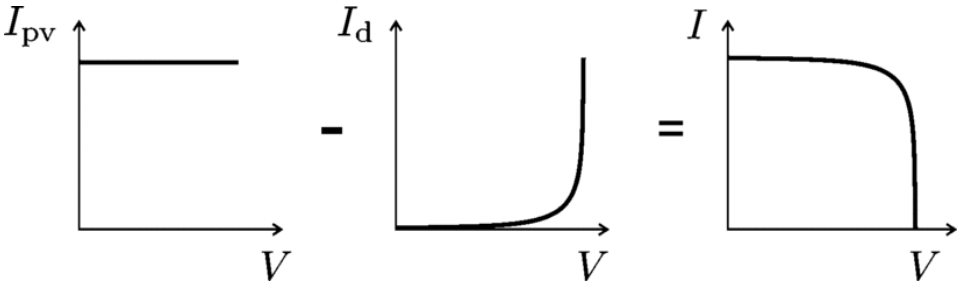

Figure 3.3: Decomposed characteristic IV curve of ideal pv cell. The net cell current I is composed by the light-generated current I_{pv} and the diode current I_d [20].

3.1 Ideal PV Cell

The equivalent circuit model of an ideal pv cell is shown in figure 3.2. It consists of a current source and a diode. The IV curve is mathematically described by equation 3.1:

$$I = I_{pv,cell} - \underbrace{I_{0,cell}\left[exp\left(\frac{qV}{akT}\right) - 1\right]}_{I_d\text{, Shockley diode equation}} \tag{3.1}$$

where $I_{pv,cell}$ is the current generated by the incident light, I_d is the Shockley diode equation, $I_0, cell$ is the reverse saturation current of the diode, T is the operating temperature of the pv cell and a is the diode ideality constant [20]. k and q are respectively the Boltzmann constant and the electron charge. Figure 3.3 shows the different components of equation 3.1.

3.2 Parameters

The following parameters are used to describe a pv module:

1. *Open-Circuit Voltage, V_{oc}:*
   The open-circuit voltage is the maximum voltage from a pv cell, occurring when the net current through the device is zero. The open-circuit voltage is indicated in the bottom right corner of figure 3.1.

2. *Short-Circuit Current, I_{sc}*
   The short-circuit current is the maximum current from a pv cell, occurring when the voltage across the terminals is zero. The short-circuit current is indicated in the upper left corner of figure 3.1.

3. *Maximum Power Point, MPP*
   The maximum power point is the operating point on the IV curve which yields the highest possible power output. The current and voltage at this point is referred to as I_{mp} and V_{mp}, respectively. The Maximum Power Point (MPP) is indicated at the knee of the IV curve in figure 3.1.

4. *Mismatch Losses*
   When connected in series, the current in a pv string is limited by the weakest cell in the string [21]. Thus, if the current of a single cell is reduced due to eg. partial shading, the current is reduced for all cells in the series connection. In addition, the weaker cell will dissipate some of the power generated in the other cells, which will cause heating and possible damage of the array [22]. Consequently, all the pv cells in a string should ideally operate under the same conditions to prevent damage and maximize the efficiency. Mismatch losses can also occur due to physical imperfections in the cells. To limit the scope of the thesis, only mismatch losses caused by different irradiation and ambient temperature are considered. Furthermore it is assumed that all cells in a string operate under the same temperature and irradiance.

5. *Maximum Power Point Tracking, MPPT*
   From figure 3.1 it is evident that a pv module has a single maximum power point for a given set of operating conditions. Maximum Power Point Tracking is the process of adjusting the terminal voltage of the module so that the maximum available power is extracted.

Chapter 4

PV Inverters

This chapter presents general pv inverter requirements. Main aspects are the different inverter families for pv applications, function blocks and requirements. In addition, the grid side control of inverters is briefly introduced. Emphasis is on large-scale grid connected inverters.

4.1 Topologies

Five inverter families can be defined related to the different configurations of the pv system: Central inverters, string inverters, multistring inverters, ac module inverters and cascaded inverters [1]. The different configurations are shown in figure 4.1. The central inverters have an advantage in the simplicity of the configuration and reduced cost. However the energy yield is low because the entire plant must operate with a single centralized MPPT for this configuration. This in turn, can lead to substantial mismatch losses. The cascaded and multistring topologies allow for independent MPPT. This increased energy yield comes at the price of increased system cost and complexity. The cascaded topologies are best suited for medium and large grid connected pv systems because the large number of converters connected in series allow for high power and/or voltage. Thus in this thesis attention is turned to these type of topologies.

4.1.1 Modular Multilevel Converter

The modular multilevel converter is suitable for operation as a multi-string inverter and cascaded inverter. Central inverter is possible as well, but it is not considered due to the substantial mismatch losses that are likely to occur with a single MPP tracker.

4.1.2 Cascaded H-bridge Inverter

Among the modular and/or cascaded inverters, the cascaded H-bridge inverter is the most frequently reported converter type for pv applications as of today [1], [2], [3]. A brief

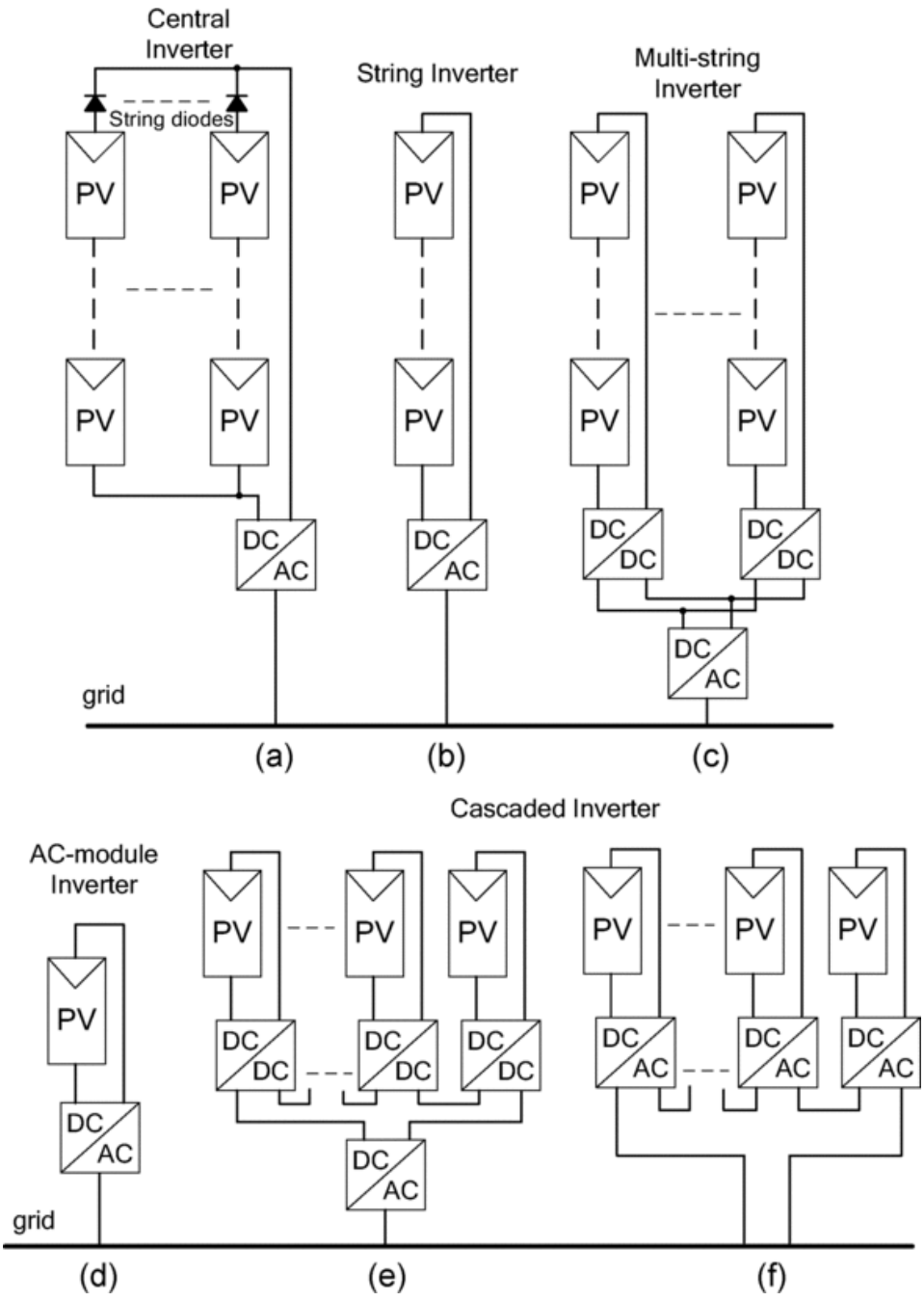

Figure 4.1: Possible pv system configurations: (a) Central inverter. (b) String inverter. (c) Multi-string inverter. (d) AC-module inverter. (e) Cascaded dc/dc converter. (f) Cascaded dc/ac inverter. [1]

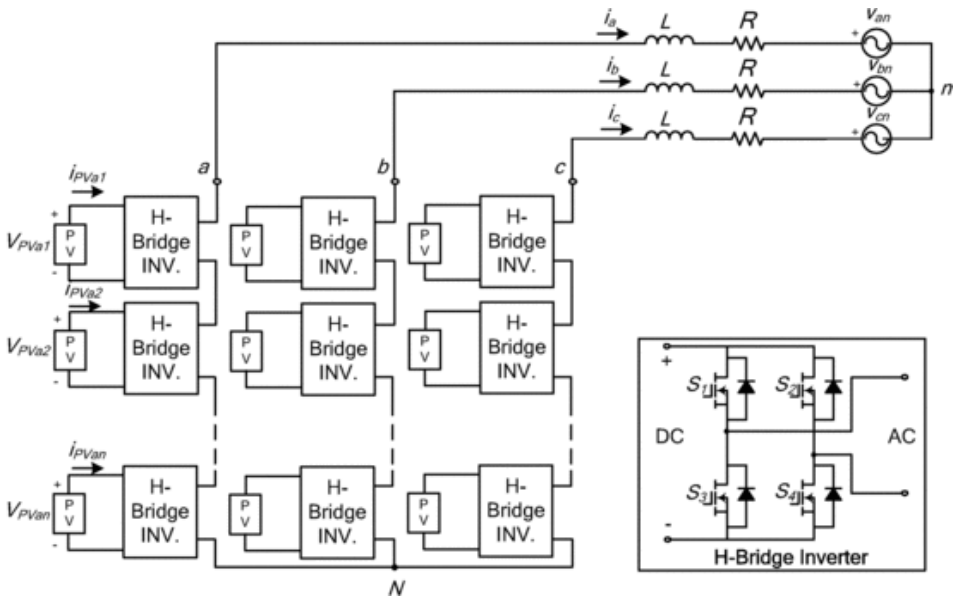

Figure 4.2: Cascaded H-bridge converter for pv applications [1]

introduction to its topology is therefore included in order to make comparisons to the Modular Multilevel Converter. With reference to figure 4.1, the cascaded H-bridge inverter is suitable for a cascaded dc-ac topology. Figure 4.2 shows a common configuration, as presented in [1]. Each phase of the converter consists of n H-bridge modules connected in series. The dc link of each module is fed by a string of pv panels. The cascaded H-bridge offers high modularity and scalability, easy implementation of redundancy and high quality of output voltage. Another distinct advantage is the implementation of MPP tracking in the H-bridge modules. This way the additional dc-dc stage which is necessary for MPPT in cascaded dc-dc converters configuration can be excluded.

4.2 Function Blocks

All pv converters share a set of common features. By focusing on the aspects concerning power electronics, ie. ignoring additional features such as communication, safety functions and monitoring, five basic functions can be identified [5]:

1. *Grid interface*
   This is the primary function block of the inverter. Traditionally this is achieved with a two-level voltage source inverter and a transformer operating at grid frequency.

2. *MPPT for the dc input*
   The extracted power from a pv system varies with the temperature, irradiation and shading conditions. In order to maximize the power output, the inverter should control the dc voltage in order for the pv modules to operate at their maximum

power point. For multilevel topologies, this can be achieved by an additional dc-dc stage, or directly in the submodules.

3. *Change of the voltage amplitude*
   The pv system must deliver a voltage that is greater than the peak value of the grid voltage. This can be done with a transformer or by a step up dc-dc stage.

4. *Power decoupling between dc- and ac side*
   The power fluctuations between dc and ac side of the inverter must be decoupled by an energy storage. Making a dc link with electrolytic capacitors is most common. For the MMC there is not one single capacitor, but rather the capacitance is divided between the submodules.

5. *Galvanic isolation between input and output*
   Traditionally galvanic isolation have been achieved by the use of transformers operating at grid frequency. This entails several drawbacks such as high cost, high weight, additional losses and a non-unity power factor. Instead the galvanic isolation can be provided with high frequency transformers, or left out altogether. However, due to the operating principle of the MMC, ie. floating capacitors in the submodules, there should be galvanic isolation between the pv arrays and the MMC. This can be obtained by using a dc-dc converter with galvanic isolation (eg. flyback converter) in the MPPT stage.

4.3 Requirements

According to [23] the next generation utility-scale pv inverters are expected to meet and demonstrate the following requirements, merits and functions:

A) Higher Reliability Target
Todays solar panels are expected to perform well for more than 25 years. The reliability of a pv system is dependent on the solar farm architecture. Statistically, centralized architecture is considered more reliable than distributed due to less part count and easier maintenance. On the other hand distributed structures offer easy scalability. In addition, redundancy is easier to implement in distributed systems, which reduces the potential effects of individual failures. Consequently modular and redundant topologies, such as the cascaded H-bridge and the MMC, are considered very interesting topologies in terms of increasing the reliability for pv systems.

B) High Power Conversion Efficiency and Performance Ratio
Generally distributed structures will offer higher energy yield from the individual pv modules than centralized structures due to the possibility of implementing individual maximum power point tracking in each string. The performance ratio of a pv system is defined to be the solar energy actually fed into the grid to the solar power theoretically available. In general the power conversion efficiency for future pv inverters should be above 98%. This favors multilevel topologies with their low switching frequency and reduced need for filters because of the harmonic performance.

C) Power Quality and Grid Support Functionalities

As mentioned in chapter 3 the power production from pv modules is highly dependent on temperature and irradiance, making it inherently non-dispatchable. To further improve the penetration of solar power generation, pv systems should provide ancillary services such as enhancing the grid reliability, improving the power quality and support grid voltage and frequency stability [24]. The power peaking capacity can be improved by implementing energy storage units. This way, the power produced during light conditions can be stored and released at peak load improving the reliability of the power supply.

4.4 Control of Grid Connected Inverters

The control tasks of a grid connected inverter can be divided in two parts: (1) The input side primarily tasked with extracting the maximum power from the pv modules. (2) Grid side controller tasked with control of active and reactive power, ensuring high quality of injected power and maintaining synchronization with the grid [25].

Traditionally the control strategy applied to the grid-side converter consists mainly of two cascaded loops. Usually, there is a fast internal current loop, which regulates the grid current, and an external voltage loop, which controls the dc-link voltage. The current loop is responsible for power quality issues and current protection; thus, harmonic compensation and dynamics are the important properties of the current controller. The dc-link voltage controller is designed for balancing the power flow in the system. Usually, the design of this controller aims for system stability having slow dynamics [25]. Control system with cascaded loops is further elaborated on in section 7.1.1

Model Predictive Control (MPC) is another possible control system for grid connection of the MMC. As the model predictive controller handles non-linear constraints it can also incorporate the MPPT stage. MPC is further elaborated on in section 7.1.2.

Part II

Method

Chapter 5

Modelling of Modular Multilevel Converter

Parts of the information in this chapter is based on the project thesis presented by the author in fall of 2014. It is reproduced here for completeness

This chapter presents a mathematical model of the MMC. Furthermore a simulation model is implemented in the Matlab/Simulink environment, using the SimPowerSystems toolbox. The simulation model includes a modified Level-Shifted PWM scheme, capacitor voltage balancing and suppression of circulating currents.

5.1 Mathematical Model of Modular Multilevel Converter

In this section the basic mathematical equations for a three phase MMC are presented. With reference to figure 2.1, the MMC is modelled as a dc-ac converter connected to the grid, as is the case for pv inverters. The grid is modelled by three sets of inductors (L), resistors (R) and a voltage source (e_j) connected in series. As mentioned in section 2.2, the capacitor voltage of each cell is ideally V_{dc}/n. Assuming this holds and neglecting the voltage loss across the arm inductance and resistance, the phase voltage can be expressed by:

$$v_j = \frac{n_{lowj} - n_{upj}}{2n} V_{dc} \quad , j = a, b, c \tag{5.1}$$

where n_{lowj} and n_{upj} are the number of cells inserted in the lower and upper arm of phase j respectively. Since the voltage across each leg must equal the dc link voltage, the following must hold (reiterating equation 2.1 for the sake of providing a complete model):

$$n = n_{lowj} + n_{upj} \tag{5.2}$$

Furthermore the upper and lower arm currents are given by [9]:

$$i_{upj} = \frac{I_{dc}}{3} + \frac{i_j}{2} + i_{circj} \tag{5.3a}$$

$$i_{lowj} = \frac{I_{dc}}{3} - \frac{i_j}{2} + i_{circj} \tag{5.3b}$$

Where I_{dc} is the dc link current, i_{circj} is the circulating current within phase j and i_{upj} and i_{lowj} is the ac-side current of upper and lower arm of phase j, respectively. Thus the arm currents consist of three components with different frequencies, namely:

1. I_{dc}, the dc offset, having zero frequency.
2. i_j, the phase current transferring power to the load at the fundamental frequency.
3. i_{circ}, current circulating at two times the fundamental frequency, caused by the voltage difference between the upper and lower arm.

From equation 5.3, it is evident that the phase components of i_{upj} and i_{lowj} are in counter phase. Consequently the magnetic fluxes of the phase currents in the upper and lower arm will cancel, meaning that the inductor only will present an inductance to the circulating current.

By respectively adding and subtracting equations 5.3a and 5.3b, expressions for the circulating current and the phase current is obtained:

$$i_{circj} = \frac{i_{upj} + i_{lowj}}{2} - \frac{I_{dc}}{3} \tag{5.4}$$

$$i_j = i_{upj} - i_{lowj} \tag{5.5}$$

By inspecting figure 2.1, equation 5.5 is in coherence with Kirchoffs current law. By also employing Kirchoffs voltage law the relation between the dc and ac side voltage for upper and lower arm is found:

$$\frac{V_{dc}}{2} = v_{upj} + L_1\frac{di_{upj}}{dt} + R_1 i_{upj} + Ri_j + L\frac{di_j}{dt} + e_j \tag{5.6a}$$

$$\frac{V_{dc}}{2} = v_{lowj} + L_1\frac{di_{lowj}}{dt} + R_1 i_{lowj} - Ri_j - L\frac{di_j}{dt} - e_j \tag{5.6b}$$

5.2 Modified Level-Shifted Pulse Width Modulation

Generally, Level-Shifted Pulse Width Modulation (LS-PWM) requires n identical triangular waveforms with amplitude 1/n displaced equally with respect to the ordinate axis.

As mentioned in section 2.4, multicarrier methods requires absolute synchronization between all carriers. To avoid this challenge altogether, [13] proposes a modified LS-PWM strategy with only one carrier. The scheme is reproduced here. Only one triangular carrier with amplitude 1/n is used. Instead the reference wave itself is shifted so that it always lies

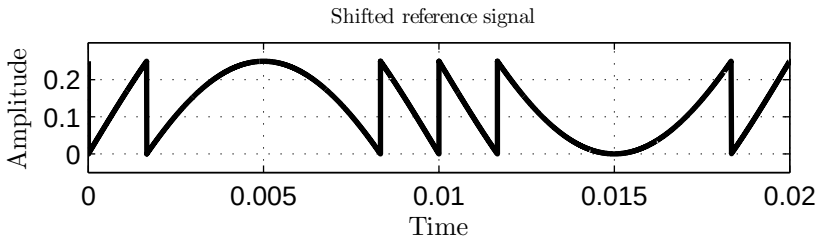

Figure 5.1: Reference signal for modified LS-PWM

Magnitude of modulating wave	Shift required	No. of cells turned ON	No. of cells turned OFF	No of cells in PWM mode
-0.5 to -0.25	0.5	0	3	1
-0.25 to 0	0.25	1	2	1
0 to 0.25	0	2	1	1
0.25 to 0.5	-0.25	3	0	1

Table 5.1: Necessary shift of the modulating waveform for modified Level-Shifted PWM, and its effect on the cells. At any instant, only one cell per arm is operating in PWM mode.

within the triangular carrier. The necessary shift for an arm with n=4 submodules is given in table 5.1. In figure 5.1, the resulting reference waveform after it has been brought inside the single carrier is provided. Furthermore, by adding an appropriate offset, the switching frequency harmonics of the upper and lower arm cancel each other. The offset is given by:

$$V_{offset} = \frac{1}{2}\left(0.25 - v_{max} - v_{min}\right) \tag{5.7}$$

where v_{max} and v_{min} is the maximum and minimum values in the given switching cycle, whilst the factor 0.25 is a result of the carrier height (1/n). Since there is only one carrier, this modified LS-PWM technique requires a balancing algorithm to determine the state of each submodule (ie. inserted, bypassed or PWM).

Implementation of the modified LS-PWM is included in appendix A.

5.3 Balancing Algorithm

Capacitor voltage balancing is vital for proper operation of the MMC. The balancing algorithm works in the following way: Prior to switching, the submodules are sorted in terms of their capacitor voltage. If the arm current is positive (negative), the submodule with the lowest (highest) voltage is inserted. The balance between the upper and lower arm can be adjusted by changing the angle of the reference in one of the arms. This will cause a difference in the power flow of the two arms, and they will become balanced. Power flow in the legs can be adjusted by adding a dc offset in the current. In all cases, the balancing requires knowledge about the capacitor voltages. As the number of submodules increases it becomes desirable, both technically and economically, to avoid measurements on every

submodule. Instead the capacitor voltages can be estimated based on the arm currents. In [10] an adaptive observer for the capacitor voltages is demonstrated. It can be considered as a software sensor. The principle is demonstrated here. The voltage across a capacitor is given by:

$$\begin{aligned} i_c &= C\frac{dv_c}{dt} \\ \Rightarrow \int_{v_c(t_1)}^{v_c(t_2)} dv_c &= \frac{1}{C}\int_{t_1}^{t_2} i_c(t)dt \\ \Rightarrow v_c(t_2) - v_c(t_1) &= \frac{1}{C}\int_{t_1}^{t_2} i_c(t)dt \end{aligned} \tag{5.8}$$

Where $t_2 - t_1 = \Delta t$ is the time between two consecutive switching instants, and i_c is the current through the submodule capacitor. In the case of the MMC, i_c is equal to the arm current when the submodule is inserted, and zero when it is bypassed. By inserting the arm currents from equation 5.3, the change in voltage for a submodule capacitor between two switching instants can be estimated:

$$\Delta v_{cup} = v_{cupi}(t_2) - v_{cup,i}(t_1) = \frac{1}{C}\int_{t_1}^{t_2}\left[\frac{I_{dc}}{3} + \frac{i_j}{2} + i_{circ}\right]dt \tag{5.9a}$$

$$\Delta v_{clow} = v_{clow,i}(t_2) - v_{clow,i}(t_1) = \frac{1}{C}\int_{t_1}^{t_2}\left[\frac{I_{dc}}{3} - \frac{i_j}{2} + i_{circ}\right]dt \tag{5.9b}$$

Implementation of the balancing algorithm is included in appendix A.

5.4 Third Harmonic Injection

By injecting a third harmonic distortion in the reference signal, the dc bus utilization can be increased without resorting to overmodulation (ie. increasing the modulation index above one) [14]. As the third harmonic components are cophasal in a three phase system, no voltage difference exist between the phases. Consequently all triplen harmonics are eliminated from the line-to-line voltage waveforms [26]. With the inclusion of a third harmonic component, the reference signal y_{ref} becomes:

$$y_{ref} = \sin(x) + A\sin(3x) \tag{5.10}$$

An analytical approach to determining the optimal value for A is provided in [26]. This is reproduced here:

The extremal points of y_{ref} are found by differentiating equation 5.10 with respect to x, and equating to zero:

$$\frac{dy}{dx} = \cos(x) + 3A\cos(3x) = 0 \tag{5.11}$$

By employing the following trigonometric identity, $\cos(3x) = 4\cos^3(x) - 3\cos(x)$, equation 5.11 can be expressed as follows:

$$[12A\cos^2(x) - 9A + 1]\cos(x) = 0 \tag{5.12}$$

By solving 5.12 for x, the angles for which the extremal points occur are found:

$$\cos(x) = 0 \quad \wedge \quad \cos(x) = \left(\frac{9A-1}{12A}\right)^{\frac{1}{2}} \tag{5.13}$$

Which yield:

$$\sin(x) = 1 \quad \wedge \quad \sin(x) = \left(\frac{1+3A}{12A}\right)^{\frac{1}{2}} \tag{5.14}$$

Where the latter is found by utilizing that $\sin^2(x)+\cos^2(x) = 1$. By using the trigonometric identity $\sin(3x) = 3\sin(x) - 4\sin^3(x)$, y_{ref} given in equation 5.10 may be expressed:

$$y_{ref} = (1+3A)\sin(x) - 4A\sin^3(x) \tag{5.15}$$

Inserting the expressions for $\sin(x)$ obtained in 5.14, the peak value of y_{ref} ($\hat{y}_{ref}$) can be found:

$$\hat{y}_{ref} = 1 - a \quad \wedge \quad \hat{y}_{ref} = 8A\left(\frac{1+3A}{12A}\right)^{\frac{3}{2}} \tag{5.16}$$

The optimal value for A is recognized as that which minimizes $\hat{y}_{ref}$. This is found by differentiating 5.16 with respect to A, and equating to zero:

$$\frac{d\hat{y}_{ref}}{dA} = \left(\frac{1+3A}{12A}\right)^{\frac{1}{2}}\left(2 - \frac{1}{3A}\right) \tag{5.17}$$

Which yield:

$$\hat{y}_{ref} = -\frac{1}{3} \quad \wedge \quad \hat{y}_{ref} = \frac{1}{6} \tag{5.18}$$

As increasing $\hat{y}_{ref}$ above 1 corresponds to over modulation, it is obvious from equation 5.16 that A must be greater than zero. Thus the optimal value for A is 1/6, and the reference signal becomes:

$$y_{ref} = \sin(x) + \frac{1}{6}\sin(3x) \tag{5.19}$$

5.5 Suppression of Circulating Currents

A distinct feature of the MMC is currents circulating within the converter. They are given by equation 5.4, and circulates at two times the fundamental frequency. Furthermore, the circulating currents are not seen on the outside of the converter, but cause increased resistive losses and tear within the converter if not suppressed. For medium and high power applications, for which the MMC is intended, the losses can be substantial. Several proposals for circulating current suppression schemes are proposed in literature. In [17],

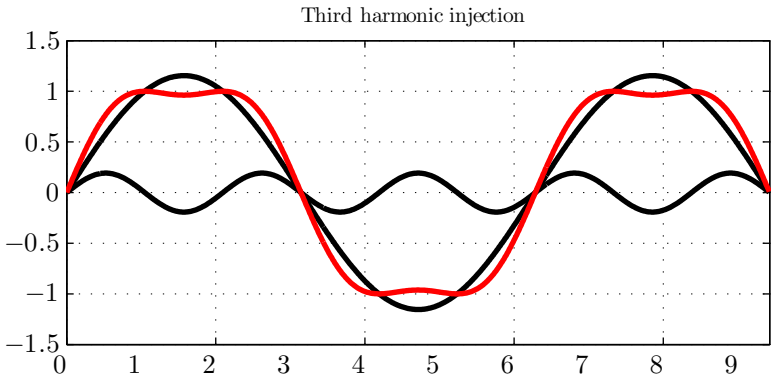

Figure 5.2: Reference signal with injection of third harmonic distortion.

a repetitive control scheme which fully eliminates the second order harmonic in the arm currents is proposed. In this thesis a simpler scheme based on adjusting the modulation indices for the upper and lower arm reference signals are implemented [16]. The correction factor is determined by the instantaneous sum of capacitor voltages in an arm and the dc bus, as given in equation 5.20.

$$m_{ji} = \frac{V_{dc}}{\sum_1^n V_{cap,ji}} \tag{5.20}$$

Where $j = \{a, b, c\}$ denotes phase, $i = \{up, low\}$ denotes arm, m is the modulation index, and V_{cap} denotes capacitor voltage. This way the voltages produced at points A_1 and A_2 in figure 2.1 are always close to a fundamental sine wave irrespective of the fluctuations of the capacitor voltages in the arms.

The implementation in Simulink of this circulating current suppression scheme is included in appendix A.

Chapter 6

Modelling of PV Devices

6.1 Mathematical model of PV devices

Several models for pv modules are presented in literature. The simplest is the ideal model introduced in section 3.1. The ideal model is simple and requires little computational time. However, it does not represent the actual solar cell IV characteristic with sufficient accuracy for engineering analysis. Through observations of the solar cell terminal behaviour under various operating conditions additional parameters have been added. The additional parameters are a series and a parallel resistance (R_s and R_p respectively). The latter accounts for leakage current to the ground. In practical devices devices the series resistance is low and the parallel resistance is high. With the inclusion of these resistances the equivalent circuit model becomes as shown in figure 6.1, and the mathematical IV characteristic becomes:

$$I = I_{pv} - I_0 \left[exp\left(\frac{V + R_s I}{V_t a} \right) - 1 \right] - \frac{V + R_s I}{R_p} \tag{6.1}$$

The last term in equation 6.1 is the current through the parallel resistance, ie. the leakage current to the ground [22]. The parameters I_{pv}, V_t, I_0 and a will be explained shortly.

I_{pv}, light generated current As stated in chapter 3, a solar cell creates a current upon exposure to light. This light generated current, I_{pv} is linearly dependent on the solar irradiation, G. In addition it is influenced by the cells operating temperature in the following manner:

$$I_{pv} = (I_{pv,n} + K_i[T - T_n]) \frac{G}{G_n} \tag{6.2}$$

In which K_i is the short circuit current/temperature coefficient which represents the rate of change of the short-circuit current with respect to the temperature, G is the irradiance reaching the surface of the module, and the subscript *n* denotes nominal conditions (ie. T=25°C and G=1000W/m^{2}C). The nominal light generated current is given by:

$$I_{pv,n} = \frac{R_s + R_p}{R_p} I_{sc,n} \tag{6.3}$$

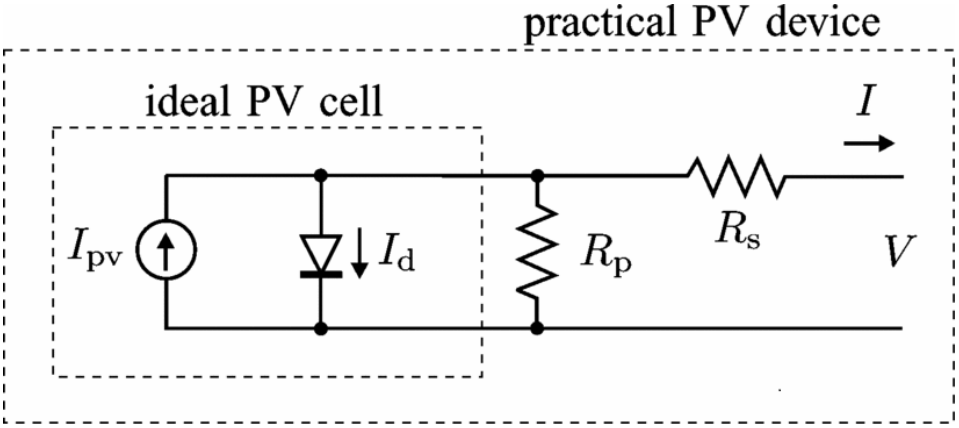

Figure 6.1: Ideal and practical model of PV device [20]

V_t, thermal voltage The thermal voltage of a pv array with N_s cells connected in series is given by:

$$V_t = \frac{N_s k T}{q} \tag{6.4}$$

I_0, diode reverse saturation current The diode saturation current, I_0, depends on the temperature as follows:

$$I_0 = I_{0,n} \left(\frac{T_n}{T} \right)^3 exp \left[\frac{qE_g}{ak} \left(\frac{1}{T_n} - \frac{1}{T} \right) \right] \tag{6.5}$$

In which E_g is the semiconductor band gap energy (E_g=1.12 eV for polycrystalline Si at 25°). The nominal saturation current, $I_{0,n}$, can be found by inserting the open circuit conditions in equation 6.1, which yields:

$$I_{0,n} = \frac{I_{sc,n}}{exp \left[\frac{V_{oc,n}}{aV_t} \right] - 1} \tag{6.6}$$

An analytical expression for the bandgap energy E_g is provided in [27]:

$$E_g = 1.16 - 7.02 * 10^-4 \left(\frac{T^2}{T - 1108} \right) \tag{6.7}$$

Equation 6.5 is known to display some model errors, especially around V_{oc}. The expression for the diode reverse saturation current can be improved by including the current and voltage coefficients K_i and K_v, which are usually provided in commercial data sheets:

$$I_0 = \frac{I_{sc,n} + K_1 \Delta_T}{exp((V_{oc,n} + K_V \Delta_T)/aV_t) - 1} \tag{6.8}$$

Symbol	Unit	Description
q	C	Electron charge
k	J/K	Boltzman constant
T	K	Temperature of the p-n junction
I_{pv}	A	Photovoltaic current
I_0	A	Saturation current
V_t	V	Thermal voltage
R_s	Ω	Equivalent series resistance
R_p	Ω	Equivalent parallel resistance
a	-	Diode ideallity constant, $1 \leq a \leq 1.5$

Table 6.1: Nomenclature used for pv modelling

a, diode ideality constant The diode ideality constant is measure of how closely the diode follows the ideal diode equation (ie. equation 3.1). A value of a=1 represents an ideal diode [28], and values between 1 and 1.5 are common [20].

The parameters for pv modelling is summarized in table 6.1.

6.2 Maximum Power Point Tracking

As stated in section 3.2 Maximum Power Point Tracking (MPPT) is the process of maximizing the power output from a pv system for a given set of conditions. From the mathematical model of a pv module it is evident that the power output from a pv system varies non-linearly with the cells operating temperature and the received irradiation. In addition, other effects such as aging, physical imperfections and partial shading influence the power output to a great extent. Thus MPPT plays an important role in maximizing the power output and efficiency of a pv system. A thorough comparative review on most of the reported MPPT techniques are presented in [29]. The techniques vary in terms of convergence rate, sensor requirements, cost, hardware implementation and simplicity. The choice of technique depends on the application at hand. Since MPPT is not the main focus of this thesis, only Perturbation and Observation (P&O), considered to be the simplest MPPT technique, will be described and used.

6.2.1 Perturbation and Observation

Perturbation and Observation (P&O) is, along with the incremental conductance method, one of the most well known hill-climbing MPPT methods. The fundamental idea of the P&O algorithm originates from the fact that the P-V characteristic of a pv system has a single global MPP. On both sides of the MPP the power is monotonously decreasing. The classical P&O algorithm works by periodically varying the reference value used to control the MPPT converter by a fixed factor ΔV_{ref} [30]. The power extracted after the change in voltage is then compared to that of the previous perturbation. If the pv power output increases, the perturbation is continued in the same direction. If not, the perturbation direc-

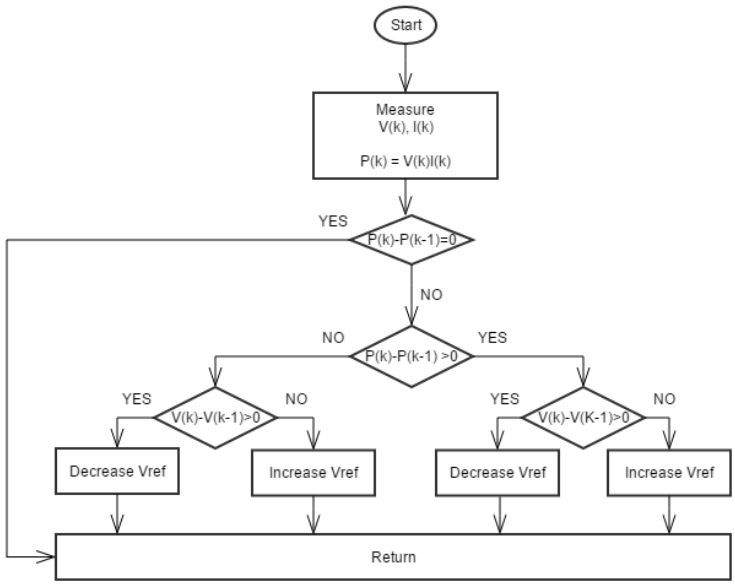

Figure 6.2: Flow chart for Perturb and Observe algorithm

tion is reversed. This way, the operating point of the pv system will gradually approach the MPP and oscillate around it at steady state. In its simplest form, the P&O algorithm uses a fixed step change for every perturbation. Better performance can be achieved by using a dynamic step value. This is beyond the scope of this thesis, and constant step is used. A flow chart of the P&O algorithm is presented in figure 6.2. The main advantage of the P&O method is that it is generic ie. suitable for any pv system, require no information about the pv array, works reasonably well under most conditions, and are easily implemented on digital controllers [31]. A drawback of P&O is that, at steady state, the operating point oscillates around the MPP giving rise to the waste of some amount of available energy. Furthermore, the P&O algorithm is known to perform poor during rapidly changing atmospheric conditions [32]. The P&O algorithm is particularly bad for ramping input of irradiance. In the event of a linearly increasing solar irradiance, the MPPT algorithm is likely to experience an increase in power, regardless of perturbation direction because the power output is proportional to the irradiance.

Implementation of the Perturb and Observe algorithm in Simulink is included in appendix B.

6.3 Simulating pv Devices

The Simscape environment in Simulink includes a model for pv modules. As the main focus of the thesis is the MMC, this model was used for simulating the pv system. The temperature dependent parameters, ie. the series resistance R_s, the parallel resistance R_p,

the thermal voltage V_t, the diode saturation current I_0 and the light-generated current I_{pv}, are implemented in look-up tables. This makes the computational load of the simulations lighter, especially since R_s and R_p must be solved iteratively [20].

Chapter 7

Possible Topologies

As discussed in chapters 3 and 6, the power generation from a pv module is highly dependent on solar irradiation and temperature. In addition external factors such as partial shading from clouds and/or dirt will affect the maximum power point of the module. As the pv modules for a large scale pv farms necessarily must cover large areas, it is very unlikely to have the same operating conditions for all modules in the farm. Thus, individual MPPT is essential to maximize the power and energy yield from a large scale photovoltaic plant. With reference to figure 4.1, multi-string and cascaded inverters both allow individual MPPT and are therefore the most obvious choices of topology.

7.1 Control Structures

From the discussion of control objectives in section 2.3, it is evident that the control objectives of the MMC are intertwined. The typical control scheme is hierarchical with at least two control loops. Another interesting possibility is Model Predictive Control (MPC). Both types are presented in the following two sections.

7.1.1 Synchronous Reference Frame Control

Synchronous reference frame control is the most common control method for grid connection of inverters. In this scheme the converter is controlled using the synchronous dq reference frame to inject a controlled current into the grid. The abc phase quantities are transformed to the rotating dq reference frame by means of the Park transformation. The dq frame rotates synchronously with the grid voltage, so that control variables becomes dc values. This enables easier filtering and control, and allows for using PI controllers, as they have satisfactory behaviour when regulating dc variables [25]. Traditionally, the dc link voltage is controlled in accordance with the necessary output power. In this case, the dc link voltage is determined by the MPPT stage of the cascaded dc-dc converters. The reactive current reference (I_q^*) is set to zero to deliver power at unity power factor.

The complexity of the MMC makes tuning of the controller gains a challenge. In this thesis the tuning was done by trial and error. The cross coupling terms and feed-forward voltage loops often associated with the synchronous reference frame control are not included. The reasoning for this is that the impedance of the MMC varies during operation, making it difficult to determine the proper constants for the feed-forward loops.

7.1.2 Model Predictive Control

In [33] MPC is defined as:

> ... a form of control in which the current control action is obtained by solving, at each sampling instant, a finite horizon open-loop optimal control problem, using the current state of the plant as the initial state; the optimization yields an optimal control sequence and the first control in this sequence is applied to the plant.

Thus, an MPC algorithm predicts the future behaviour of the system and acts accordingly, making it a powerful tool for dynamic conditions. In [34] an MPC algorithm is proposed which uses a single loop to maintain the load current within acceptable limits, whilst simultaneously minimizing the capacitor voltage fluctuations and circulating currents. In addition to the circulating currents and capacitor voltage variations, the cost function accounts for the average switching frequency. A distinct advantage with an MPC controller is that it can handle non-linear constraints on both states and control variables. This means that the MPPT stage in theory can be incorporated in the cost function. One of the challenges associated with an MPC controller is choosing the right constants for the cost function.

7.1.3 Comparison

In [35] the performance of a model predictive algorithm and a conventional cascaded control system based on PI controllers for control of MMC are compared. It is found that the conventional controller performs slightly better under steady state conditions, but the model predictive controller is superior during dynamic conditions. However, the comparison is made for an MMC with N=2 submodules per arm only. The main drawback related to model predictive control of multilevel converters is computational time since the number of states, and thus computational time, increases exponentially with the number of submodules. Consequently a controller based on model prediction for MMC should be implemented with set of rules to reduce the number of possible states, as proposed in [36].

7.2 Cascaded dc-dc Converters Topology

Figure 7.1 shows a possible topology based on cascaded dc-dc converters. In figure 7.1, synchronous reference frame control is used. MPC is a viable option for this configuration as well. Each dc converter has individual MPPT, so that mismatch losses are avoided. In addition, every dc converter has a bypass switch, so that the plant can keep operating in the case of failure in one of the dc-dc stages. With cascaded dc-dc converters, the three

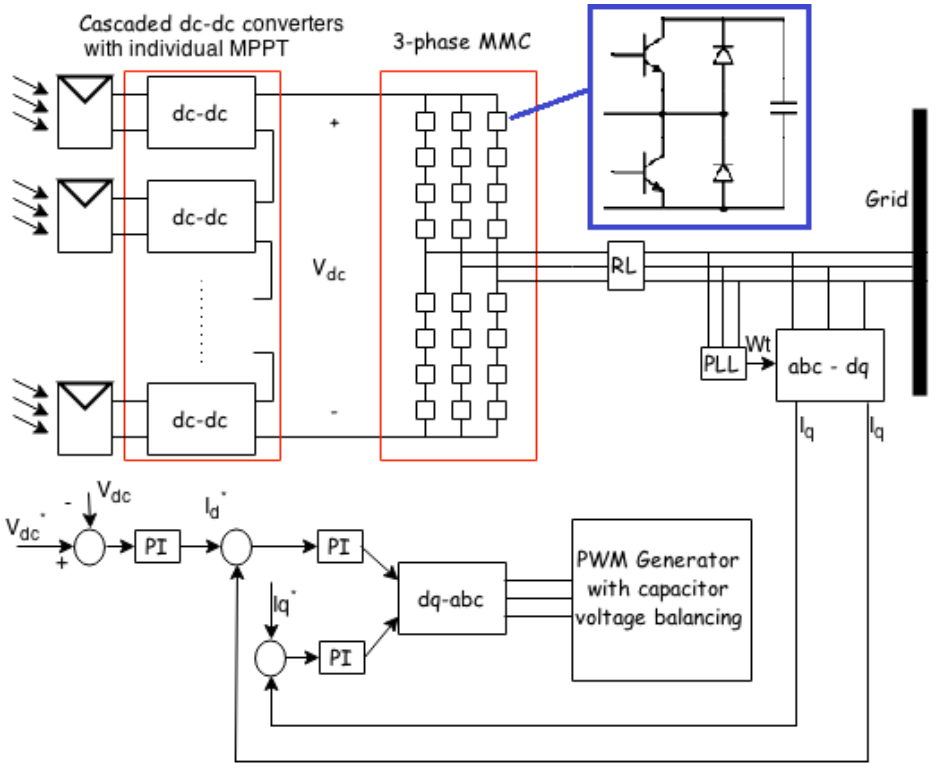

Figure 7.1: MMC based pv inverter with cascaded dc-dc converters. Grid synchronization and control is achieved with synchronous reference frame control. MPC is another option for control.

phases share the same dc link voltage. As a result, the converter will always maintain the same number of voltage levels, regardless of operating conditions and/or failure of the individual pv strings. In the event of an outage of a string due to faults or lack of irradiation, the reduction in voltage is shared equally among the submodules.

7.3 Multi-string Inverter Topology

Figure 7.2 shows a possible configuration based on a multistring inverter topology. With this topology, each pv string is connected to a single submodule. This way each submodule has a separate dc source, instead of the shared dc link of the cascaded dc-dc converters. Consequently, each submodule will receive different power depending on the operating conditions of the pv string. Multi-string topologies therefore require power imbalance compensation. Per submodule imbalance can be remedied by adjusting the on and off times of each cell. Per phase imbalance can be compensated by introducing a distortion in the voltage reference inversely proportional to the power imbalance between the phases [37]. Both synchronous reference frame control and MPC are viable options for this con-

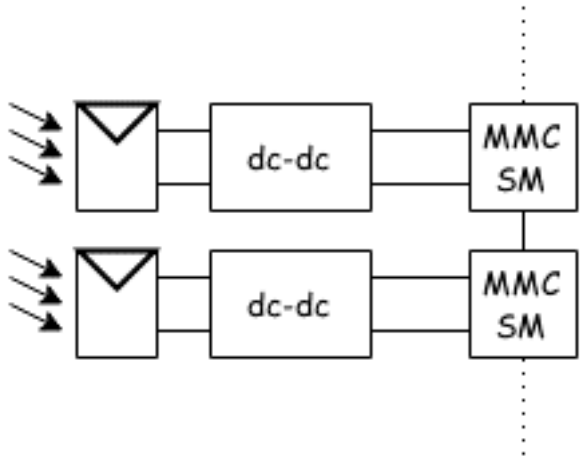

Figure 7.2: MMC based pv inverter with multi-string topology. Similar to the cascaded dc-dc design, grid synchronization can be achieved by synchronous reference frame control or MPC.

figuration.

Part III

Results, Discussion and Conclusion

Chapter 8

Simulations

This chapter presents four simulations. Simulation 1 is of the steady state behaviour of the MMC to verify that it is behaving in accordance with the theoretical model. Simulation 2 is of the circulating current suppression scheme presented in section 5.5. Simulation 3 is of a pv module with MPPT and variable irradiance and ambient temperature. Simulation 4 is of the cascaded dc-dc converter topology presented in section 7.2 with synchronous reference frame control.

8.1 Simulation 1: Steady State Waveforms of MMC

The steady state waveforms of the phase currents and phase to phase voltages of an MMC operating in open loop are shown in figures 8.1 and 8.2. The implementation of the modified PWM generator with capacitor voltage balancing for one phase is included in appendix A.

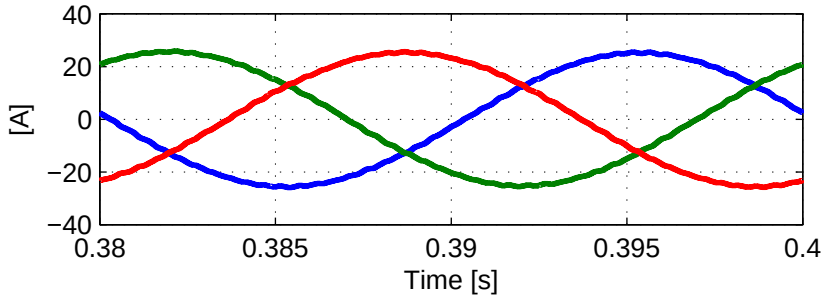

Figure 8.1: Simulation 1: Phase currents of MMC operating in steady state. The phase currents are smooth with a total harmonic distortion of 1.07%, 1.08% and 1.22% for phases a, b and c respectively

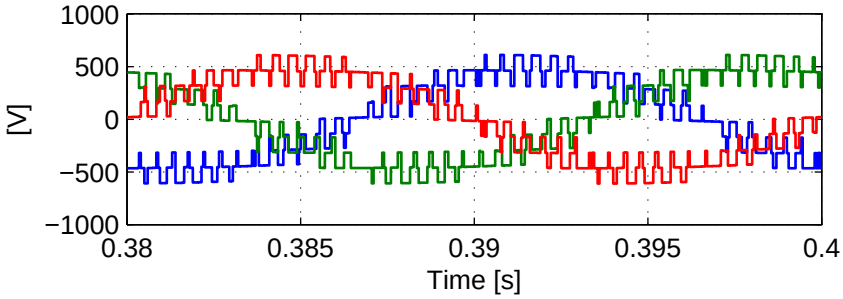

Figure 8.2: Simulation 1: Phase to phase voltages of MMC operating in steady state. The total harmonic distortion of the phase voltages are 26,11%, 25.89% and 26.03% for phase a, b and c respectively.

8.2 Simulation 2: Supression of Circulating Currents in the MMC

In this section the behaviour of the MMC with and without the circulating current suppression scheme presented in section 5.5 is simulated. The modification of the reference signal is shown in figure 8.3. Figure 8.4 shows the arm voltages with and without suppression. Figure 8.5 shows the submodule capacitor voltages of the upper arm of phase *a* with and without suppression. Table 8.1 specifies the harmonic content of the arm currents. The implementation of the suppression scheme for circulating currents is included in appendix A.

Supression	Arm currents	THD	0 Hz (dc)	100 Hz	150 Hz	200 Hz
No	I_{up}	159.39	35.03	159.23	1.91	6.36
	I_{low}	203.97	42.87	203.78	2.37	7.93
Yes	I_{up}	108.87	29.00	108.03	0.59	2.57
	I_{low}	120.09	31,73	120.03	0.38	3.01

Table 8.1: The effect of circulating current suppression. Total harmonic distortion and frequency components of upper and lower arm currents with and without modulation index adjustment for suppression of circulating currents

8.3 Simulation 3: PV Module with MPPT

The pv module used for simulating is Sun Power SPR-305-WHT with 66 modules in series and 5 in parallel. This yields a power of 100.7 kW at $G = 1000W/m^2$ and $T = 25°C$. Figure 8.6 shows the IV- and PV curves for the given module for different levels of irradiation. The pv module is connected to a detailed model of a boost converter whose duty ratio is controlled by a Perturb and Observe MPP tracker. The MPP tracker is activated after 0.3 seconds. The simulation is done with variable irradiance and ambient temperature to

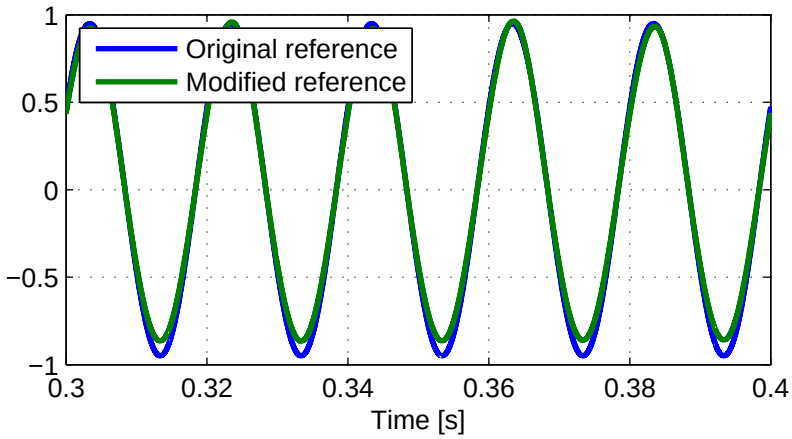

Figure 8.3: Simulation 2: Reference signal for upper arm of phase *a* after the modulation index has been altered. The modulation index becomes on average lower than without current suppression. This reduces the dc link utilization.

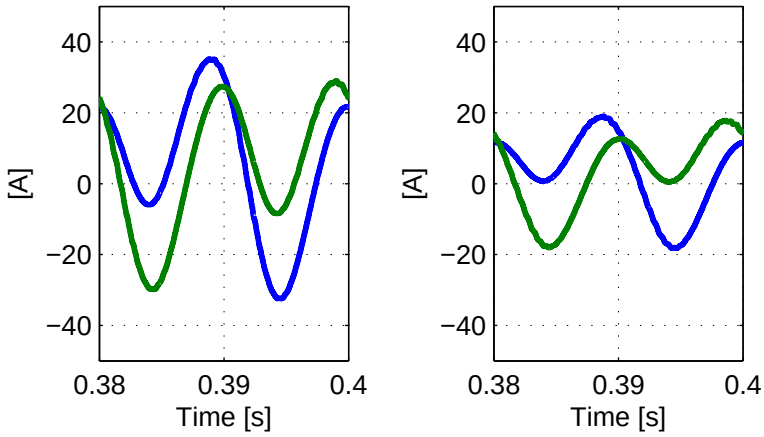

(a) Arm currents of phase a without suppression of circulating currents

(b) Arm currents of phase a with suppression of circulating currents

Figure 8.4: Simulation 2: Arm currents with and without circulating current suppression.

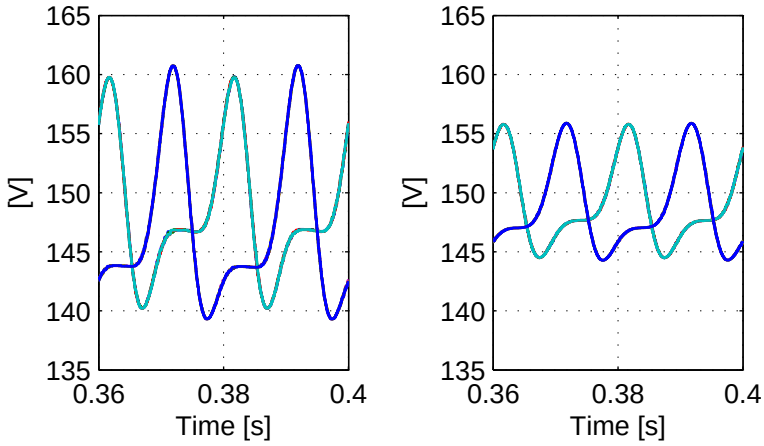

(a) Capacitor voltages without suppression of circulating currents

(b) Capacitor voltages with suppression of circulating currents

Figure 8.5: Simulation 2: Capacitor voltages with and without circulating current suppression. One fundamental cycle at steady state of the capacitor voltages with and without circulating current suppression. The capacitor voltages charge with twice the fundamental frequency, indicating that there are still considerable second order harmonics in the arm currents, even after suppression

test the MPPT algorithm from section 6.2.1. The implementation of the MPPT algorithm is included in appendix B. The input irradiance and temperature is given in figure 8.7. The resulting duty ratio is shown in figure 8.8. The array voltage and power is shown in figures 8.9 and 8.10 respectively. The pv module was simulated with a sample time of 1e-06 to give satisfactory results.

8.4 Simulation 4: Cascaded dc-dc Converters

This section presents a simulation of the system topology given in figure 7.1 of section 7.2. Due to extremely slow simulation time with the pv system connected to the MMC, a controllable voltage source was used instead. The dc link voltage is set to oscillate to mimic the behaviour of multiple pv strings with individual Perturb and Observe MPP trackers. At t=3.05 seconds a step decrease in the dc link voltage occurs to imitate failure of a dc-dc converter and the activation of a bypass switch. As was stated in section 7.1.1, the tuning of the PI regulators was done by trial and error. Implementation in Simulink of the synchronous reference frame control system is presented in appendix C.

Figure 8.11 shows the dc link voltage with a step change at t=3.05s. Figure 8.12 shows the reference signals for the PWM. Figures 8.13 and 8.14 shows the phase voltages and currents respectively. Figure 8.15 shows the capacitor voltages of phase a. Figure 8.16 shows the circulating currents of phase a.

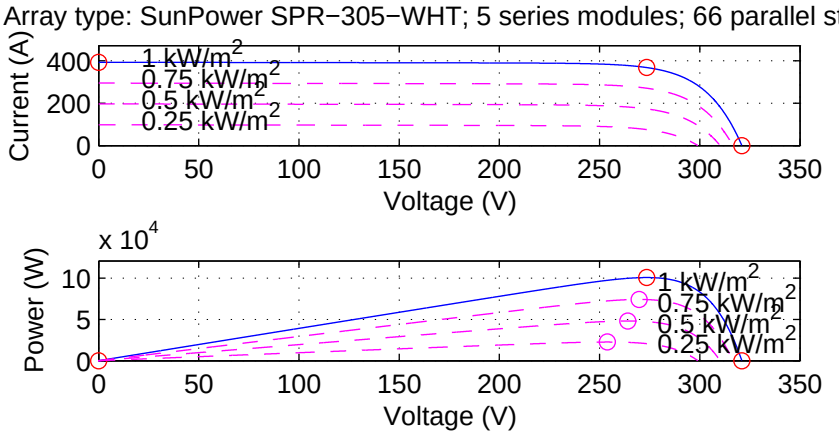

Figure 8.6: IV- and PV characteristics for SunPower SPR-305-WHT for different levels of irradiation

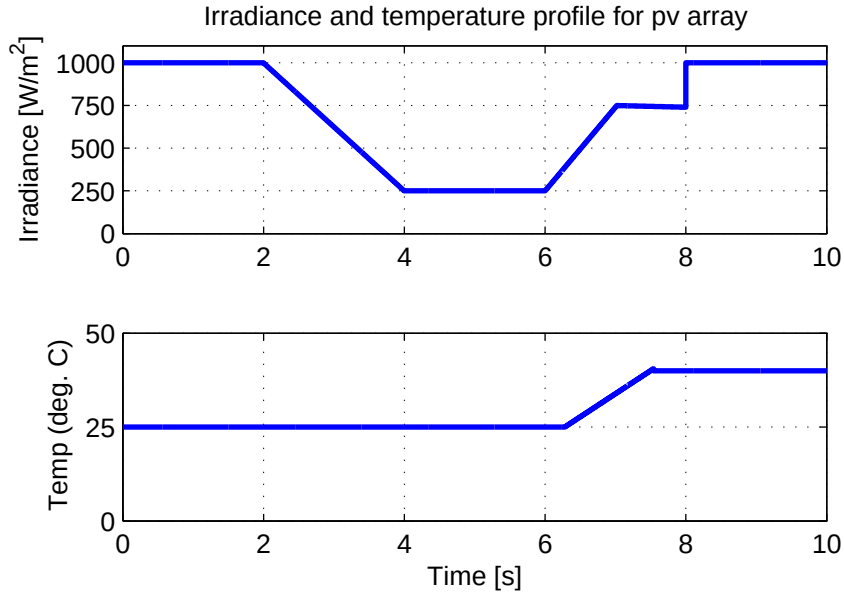

Figure 8.7: Simulation 3: Irradiance and temperature profile for simulation of PV array with MPPT

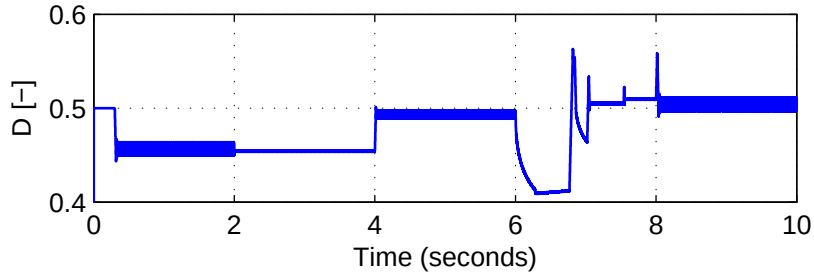

Figure 8.8: Simulation 3: Duty ratio for boost converter during simulation of pv module

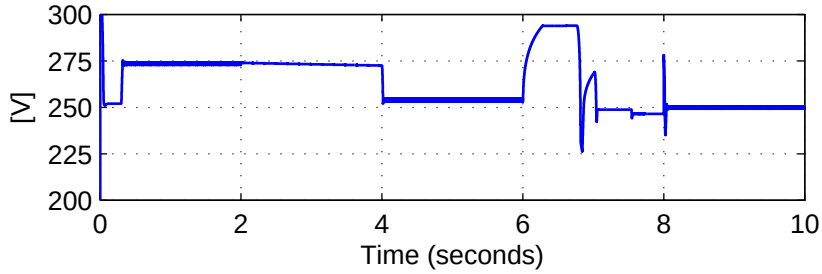

Figure 8.9: Simulation 3: Terminal voltage for pv module

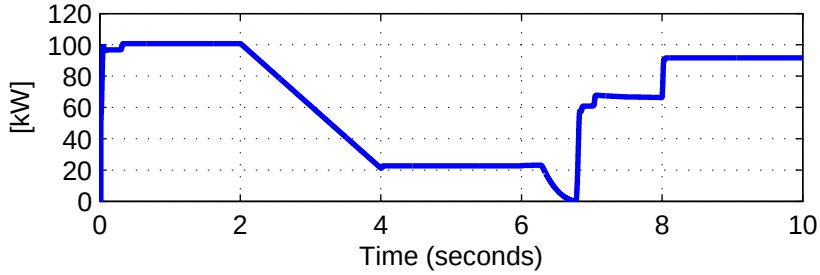

Figure 8.10: Simulation 4: Power delivered by pv module

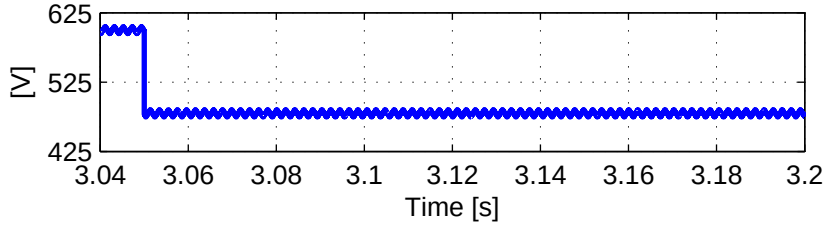

Figure 8.11: Dc link voltage, oscillating to mimic the behaviour of pv strings with MPP tracking, and with a step change at 3.05 seconds to represent the outage and bypassing of a dc-dc converter.

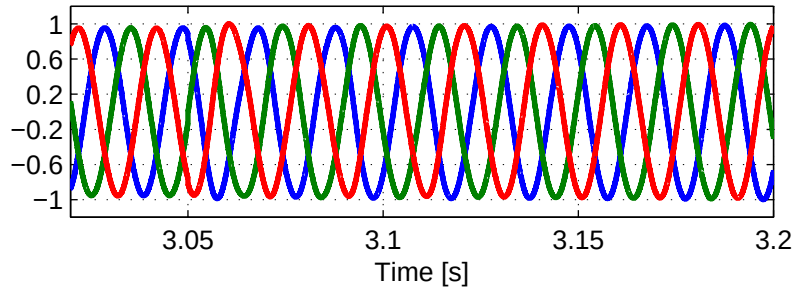

Figure 8.12: Simulation 4: Reference signal for the PWM with a step change in the dc link voltage. The amplitude increases slightly in response to the change in dc link voltage.

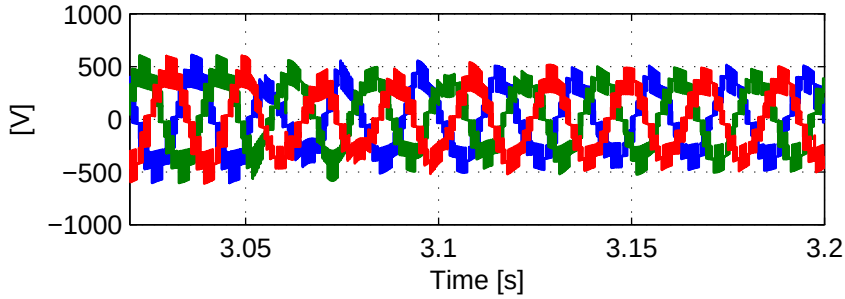

Figure 8.13: Simulation 4: Phase to phase voltages for the MMC during a step change in the dc link voltage. After an initial transient, the phase to phase voltages stabilizes at the new dc link voltage.

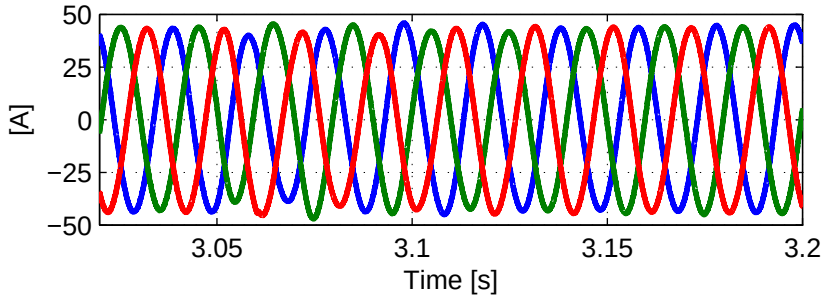

Figure 8.14: Simulation 4: Phase currents from the MMC during a step change in the dc link voltage. After an initial transient, the phase currents returns to the pre-fault state.

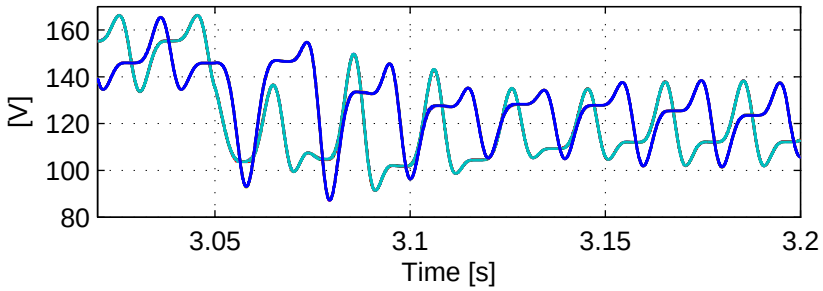

Figure 8.15: Simulation 4: Submodule capacitor voltages during a step change in the dc link voltage. After an initial transient with uneven voltage distribution among the upper and lower arm, the capacitor voltages are congregated at a new equillibrium.

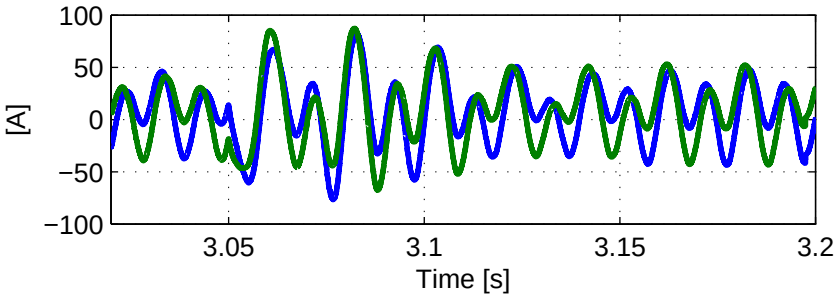

Figure 8.16: Simulation 4: Arm currents of phase a. The arm currents increase substantially in response to the step change in dc link voltage.

Chapter 9

Discussion

This chapter discusses the main findings of the thesis. Section 9.1 discusses the applicability of MMC as grid interface for pv systems. The criteria for discussion are the possible pv system configurations, function blocks and requirements given in sections 4.1, 4.2 and 4.3 respectively. Section 9.2 concerns the primary control objectives of the MMC, as presented in section 2.3. Finally, in section 9.3 the simulations of chapter 8 are discussed.

9.1 MMC as Grid Interface for pv

This section discusses the MMC as interface for a pv farm in light of the possible system configurations, function blocks and general requirements presented in chapter 4.

Section 4.1 listed five possible system topologies for grid connected pv inverters. For multilevel topologies, such as the MMC, the multi-string and cascaded system types are most interesting. Both of these allow individual MPPT, which is essential to avoid mismatch losses and maximizing the energy yield from the pv modules. Individual MPPT, along with the low switching frequency associated with multilevel converters gives a high efficiency. As was stated in section 4.3, the efficiency of future pv inverter system should be above 98%. Furthermore, the low total harmonic distortion of the output waveforms reduce the need for filters. In addition the MMC does not require a grid side transformer to reach the necessary voltage levels for grid connection This further enhances the efficiency of the system. If galvanic isolation is required, this can be provided in the dc-dc stage.

The part count of the MMC is high. However, it has no central components. This means that redundancy is easily implemented, and operation can continue in spite of individual failures. This increases the reliability of the system. In addition, the modular structure makes the system easily scalable.

In future power systems, renewable energy sources are expected to provide ancillary services, in addition to feeding power into the grid. From the mathematical model of the pv

system presented in section 6.1, it is evident that the power generation from a pv module is inherently non-dispatchable. The power peaking capability of a pv inverter system can be increased by implementing a battery storage. During light conditions, pv modules will deliver power to the battery instead of the grid. This power can be released during peak load. Another approach could be to operate the pv modules away from the MPP during normal operation. In the event of a sudden increase in load, the operating point of the modules can be moved towards the MPP. This way, some form of spinning reserve is incorporated in the pv system. However, considering the dependency on operating conditions for pv modules, this is not considered a good idea. Besides, the accumulated power loss related to always operating the pv modules away from the MPP would be substantial, making the 98% efficiency target difficult to meet.

9.2 Control of MMC

This section discusses choice of pv inverter configuration in light of submodule capacitor balancing, circulating current suppression and active and reactive power control.

9.2.1 Submodule capacitor balancing

Submodule capacitor balancing is only a concern for the cascaded system configurations. For the cascaded topologies, all submodules share the same dc link, and the balancing becomes similar to that for hvdc applications. The main difference being that the dc link voltage will vary according to the operating conditions for the pv modules. For multi-string topologies, the submodules does not share the same dc link voltage. The challenge then becomes to compensate for the power imbalance between the individual cells and phases in order to deliver symmetrical currents to the grid. Consequently the multi-string topologies require power imbalance compensation instead of capacitor voltage balancing. Both these tasks are considered similar in complexity. However, in the event of outage of a pv string, the multi-string topology will lose a voltage level in one arm, whilst in the cascaded dc-dc topology the voltage drop will be evenly shared among all submodules in the three phases. This is in favor of the cascaded dc-dc topology.

9.2.2 Circulating Current Suppression

The inner circulating currents of the MMC will cause losses and require higher rated components if not minimized. The circulating currents in an arm is caused by the voltage difference between the upper and lower arm, and the instantaneous voltage ripples of the submodule capacitors. The circulating currents will be present in both cascaded dc-dc and multi-string configurations. The cascaded H-bridge inverter presented in section 4.1.2 does not have circulating currents. Thus the circulating currents of the MMC must be fully suppressed to match the performance of the cascaded H-bridge inverter.

9.2.3 Active and Reactive Power Control

Traditionally grid synchronization and active and reactive power control is achieved with cascaded PI controllers, as explained in section 7.1.1. A challenge related to this is tuning of the PI regulators. The complex topology of the MMC makes it difficult to define a transfer function. In addition, the impedance of the MMC varies during operation, which makes it hard to determine the feed forward terms often associated with cascaded PI controllers. Another possible control strategy is model predictive control. MPC has the advantage of handling non-linear constraints on states and control variables. This means that MPPT stage can be included in the cost function. Another advantage with a model predictive controller is that it works well in dynamic conditions, as stated in section 7.1.2. With pv modules as sources, dynamic conditions are likely to occur. The main problem with a model predictive controller is the computational power required. The number of possible states in the system increase exponentially with the number of submodules. However, most studies of MPC for MMC is for hvdc applications. The number of submodules required for grid connection of pv modules is lower than that for hvdc. This makes MPC an interesting control strategy for this purpose.

9.3 Simulations

In this section the results from the simulations in chapter 8 are discussed.

9.3.1 Simulation 1: Steady State Waveforms of MMC

The steady state waveforms of the MMC are in accordance with the expected values. Four submodules per arm gives a phase to phase voltage with nine levels, as shown in figure 8.2. The total harmonic distortion of the current is 1%. For the phase to phase voltages the total harmonic distortion is 25%, the majority of which is multiples of the switching frequency with sidebands.

9.3.2 Simulation 2: Supression of Circulating Currents in the MMC

The current suppression scheme presented in section 5.5 yields very good results. It is only the modulation indices of the reference signals that are altered, as can be seen in figure 8.3. The modulation index is on average reduced with this method, meaning that the dc link voltage is not fully utilized. This is a drawback with the method. As discussed in section 5.4, the dc link utilization can be increased by injecting a third harmonic distortion in the reference. The arm currents for phase a of the MMC are plotted in figure 8.4. Fourier analysis of the signal reveals that it has three main frequency components, as seen in table 8.1: A dc-, a fundamental- and a twice the fundamental component. This is in accordance with equation 5.3 of the mathematical model presented in section 5.1. By employing the suppression scheme the total harmonic distortion of the arm currents is reduced from 159.39% to 108.87% in the upper arm and from 203.97% to 120.09% in the lower arm. As a result the peak amplitude of the arm current is substantially reduced. The reduction in second order harmonic currents also positively affects the capacitor voltage balancing, as

can be seen in figure 8.5. This further underlines the importance of suppressing the second order harmonics in the arm currents.

9.3.3 Simulation 3: PV Module with MPPT

The MPP tracking experiences trouble when both irradiance and temperature is increasing linearly simultaneously. At this time the pv voltage approaches V_{oc} and the power delivered drops to zero. More robust MPPT algorithms than the Perturb and Observe are expected to not exhibit this behaviour. Apart from this and some transients during change in operating conditions the MPPT algorithm adjusts the duty ratio of the boost converter correctly.

9.3.4 Simulation 4: Cascaded dc-dc Converters

The cascaded dc-dc inverter topology responds satisfactory to the sudden drop in dc link voltage. For the MMC the phase voltages are set by the dc link voltages, as can be seen in figure 8.13. The amplitude of the phase voltages drops the same as the dc link. As there are no transformer in this topology, and the voltage of the dc-dc stage is determined by the MPPT stage, this topology lacks the ability to change the voltage amplitude. This represents a problem if the dc link voltage drops below the grid voltage, and the direction of power is turned. A possible remedy to this is the inclusion of a energy storage unit. This way, the pv modules can supply the battery when the dc link voltage is to low, or at times of excess power. In return the energy storage can be used during the peak load hours. The phase currents are shown in figure 8.14 and stabilizes quickly after some transients. The capacitor voltages are shown in figure 8.15. In response to the sudden voltage drop, the upper and lower arms become unevenly charged. However, the balancing algorithm quickly remedies this, and after some transients the capacitor voltages stabilizes around the new equilibrium point (V_{dc}/n). The circulating currents increase substantially in response to the step change in dc link voltage. This will represent a considerable tear, or may cause destruction of the components. Consequently, a stronger current suppression scheme than the one proposed in section 5.5 will be necessary.

A weakness with this simulation is the tuning of the PI regulators based on trial and error, and the use of a controllable voltage source instead of the pv modules with MPPT as the dc link voltage.

Chapter 10

Conclusion and Further Work

10.1 Conclusion

The applicability of the Modular Multilevel Converter (MMC) for interfacing grid connected photovoltaic conversion plants has been investigated.

The MMC offers several interesting characteristics. Its modularity makes it highly scalable and enables it to meet conceptually any voltage level requirement. The high number of voltage levels yield superior harmonic performance, reducing or even eliminating the need for ac side filters. The operating principle of the MMC has been presented. Two control objectives have been identified as distinctive for the MMC. Namely capacitor voltage balancing and circulating current control. The circulating currents are not detectable outside of the converter, but can cause significant wear and losses if not minimized.

A detailed three phase 9-level simulation model was implemented in Simulink. The steady state behaviour of the model is in accordance with the theoretical model. The model includes capacitor voltage balancing and circulating current reduction. The reduction of circulating currents was done by separately adjusting the modulation indices of each arm. As a result the circulating currents were reduced. With this method the modulation indices was on average decreased. This leads to a reduction of the dc link utilization.

Photovoltaic power generation is highly dependent on operating conditions. Maximum Power Point Tracking (MPPT) is the process of adjusting the terminal voltage of the pv module to deliver the maximum available power. To avoid mismatch losses and maximize the power yield, the pv cells connected to the same MPP tracker should have the same operating conditions. For large scale pv farms, this is only possible with multiple MPP trackers.

Five system configurations was identified for pv inverters. Of these, cascaded inverter and multi-string inverter are viable options for grid connection of large-scale pv farms

with individual MPPT. For a topology based on cascaded dc-dc converters, the three phase legs share the same dc link voltage. Consequently, the inverter will always have the same number of voltage levels. For multi-string topologies, each submodule is fed by a separate pv string. Thus power imbalances between submodules and phases are inevitable. This can be remedied by power imbalance compensation. However, in the event of a pv string failure, the multi-string inverter will permanently lose a voltage level in that arm. This favors the cascaded dc-dc converter configuration. For both configurations suppression of the circulating currents is essential to minimize the losses in the inverter stage.

Synchronous Reference Frame Control (SRFC) and Model Predictive Control (MPC) have been explored as possible control strategies. MPC has the advantage of handling non-linear constraints on both states and variables. In addition it is reported to perform better than SRFC during dynamic conditions, which are likely to occur often with pv generators.

10.2 Further Work

The work in this thesis is limited to half bridge submodule topologies. With other submodule topologies, the MPPT can be performed in the submodules. This way the additional dc-dc stage can be left out. This will lower the system cost and complexity. Model Predictive Control holds properties that are interesting for this applications. With a model predictive controller, the MPPT can be included in the cost function along with the other control objectives of the MMC.

Appendices

Appendix A

Implementation of PWM and Balancing Algorithm in Simulink

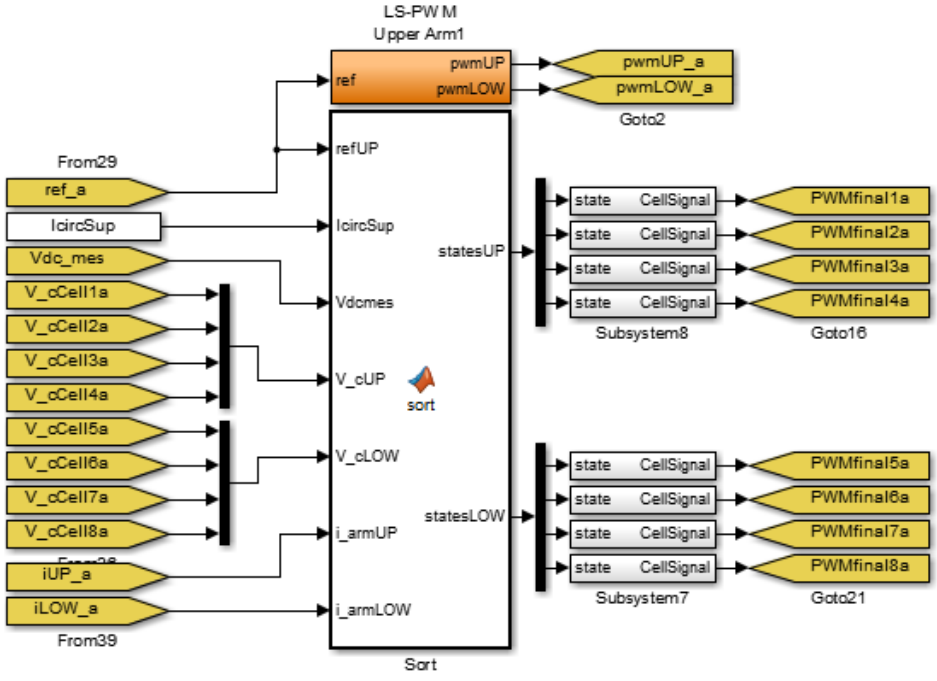

Figure A.1: Simulink diagram: PWM generator for phase a. Diagram is duplicated for phase b and c.

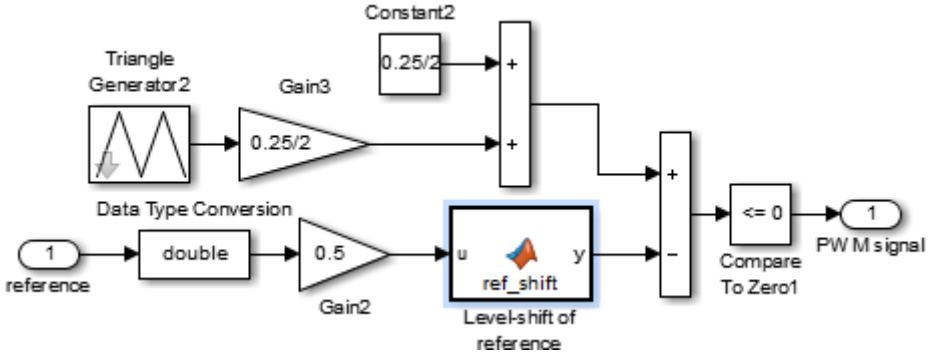

Figure A.2: Simulink diagram: Modified LS-PWM. The orange block in figure **??**

```
function y = ref_shift(u)
%#codegen
if u<=-0.25
%     shift=0.5;
    u=u+0.5;
elseif u<=0
    u=u+0.25;
%     shift=0.25;
elseif u<=0.25
    u=u;
%     shift = 0;
elseif u<=0.5
    u=u-0.25;
%     shift=-0.25;
end
y = u;
```

```
function [statesUP,statesLOW]    = sort(refUP,IcircSup,Vdcmes,...
                                        V_cUP,V_cLOW,i_armUP,i_armLOW)
%#codegen

%% Modulation index modification
mUP=1;
if(IcircSup)
mUP = Vdcmes/(V_cUP(1)+V_cUP(2)+V_cUP(3)+V_cUP(4));
if mUP>0.95
    mUP = 0.95;
elseif mUP<0.85;
    mUP = 0.85;
end
refUP = mUP*refUP;
end

%% No of inserted cells:

insertedUP=0;
```

```
if refUP<=-0.5
    insertedUP=1;
elseif refUP<=0
    insertedUP=2;
elseif refUP<=0.5
    insertedUP = 3;
elseif refUP<=1.0001
    insertedUP=4;
end

%% sorting
[~,Vsort]= sort(V_cUP);
pos=zeros(4,1);
for i=1:4
    if Vsort(i)==1
        pos(1)=i;
    elseif Vsort(i)==2
        pos(2)=i;
    elseif Vsort(i)==3
        pos(3)=i;
    elseif Vsort(i)==4
        pos(4)=i;
    end
end

%% allocating
% Each cell is assigned either bypassed (0), inserted (1)
% or PWM (2).
statesUP=zeros(4,1);
for i = 1:4
    if i_armUP>=0
        if pos(i)<insertedUP
            statesUP(i)=1;
        elseif pos(i)==insertedUP
            statesUP(i)=2;
        else
            statesUP(i)=0;
        end
    else
        if pos(i)>(5-insertedUP)
            statesUP(i)=1;
        elseif pos(i)==(5-insertedUP)
            statesUP(i)=2;
        else
            statesUP(i)=0;
        end
    end
end

%% ######################################################

% LOWER ARM
%% Modulation index modification
mLOW=1;
if(IcircSup)
mLOW = Vdcmes/(V_cLOW(1)+V_cLOW(2)+V_cLOW(3)+V_cLOW(4));
if mLOW>0.95
```

```
    mLOW = 0.95;
elseif mLOW<0.85;
    mLOW = 0.85;
end
end
%% No of inserted cells:
refLOW = -refUP*mLOW;
insertedLOW=0;
if refLOW<=-0.5
    insertedLOW=1;
elseif refLOW<=0
    insertedLOW=2;
elseif refLOW<=0.5
    insertedLOW = 3;
elseif refLOW<=1.0001
    insertedLOW=4;
end

% PWMLOW=PWMsLOW(5-insertedLOW);


%% sorting
[~,Vsort]= sort(V_cLOW);
pos=zeros(4,1);
for i=1:4
    if Vsort(i)==1
        pos(1)=i;
    elseif Vsort(i)==2
        pos(2)=i;
    elseif Vsort(i)==3
        pos(3)=i;
    elseif Vsort(i)==4
        pos(4)=i;
    end
end

%% allocating
% Each cell is assigned either bypassed (0), inserted (1)
% or PWM (2).
statesLOW=zeros(4,1);
for i = 1:4
    if i_armLOW>=0
        if pos(i)<insertedLOW
            statesLOW(i)=1;
        elseif pos(i)==insertedLOW
            statesLOW(i)=2;
        else
            statesLOW(i)=0;
        end
    else
        if pos(i)>(5-insertedLOW)
            statesLOW(i)=1;
        elseif pos(i)==(5-insertedLOW)
            statesLOW(i)=2;
        else
            statesLOW(i)=0;
        end
```

```
134         end
135     end
136     end
```

Appendix B

Implementation of MPPT in Simulink

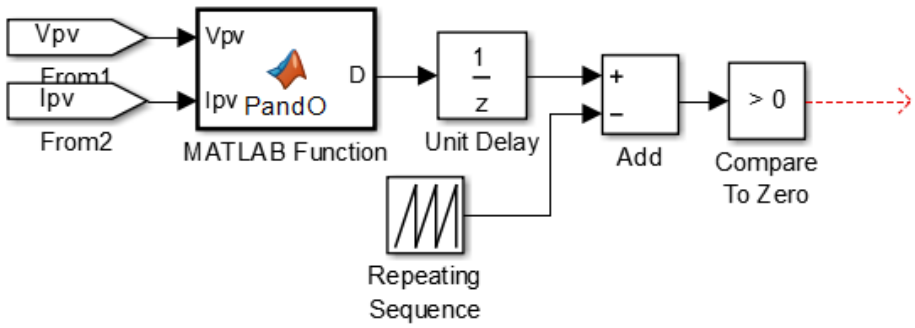

Figure B.1: Simulink diagram: MPPT

```
function D = PandO(Vpv,Ipv)
%#codegen

% Define internal values for the Duty cycle, Voltage and power
% as persistent variables
persistent Dprev Pprev Vprev

% Set initial values:
if isempty(Dprev)
    Dprev = 0.5;
    Vprev = 0;
    Pprev = 0;
```

```
13 end
14
15 % set duty cycle increment
16 deltaD = 0.0001;
17
18 % Calculate measured array power
19 Ppv = Vpv*Ipv;
20
21 % Increase/decrease duty cycle based on conditions
22 if (Ppv-Pprev) ~= 0
23     if (Ppv-Pprev) > 0
24         if (Vpv-Vprev) > 0
25             D = Dprev - deltaD;
26         else
27             D = Dprev + deltaD;
28         end
29     else
30         if (Vpv-Vprev)>0
31             D = Dprev + deltaD;
32         else
33             D = Dprev - deltaD;
34         end
35     end
36 else
37     D = Dprev;
38 end
39
40 if D >= 0.8 || D<= 0.2
41     D=Dprev;
42 end
43
44 % Update internal values
45 Dprev = D;
46 Pprev = Ppv;
47 Vprev = Vpv;
48 end
```

Appendix C

Implementation of Synchronous Reference Frame Control in Simulink

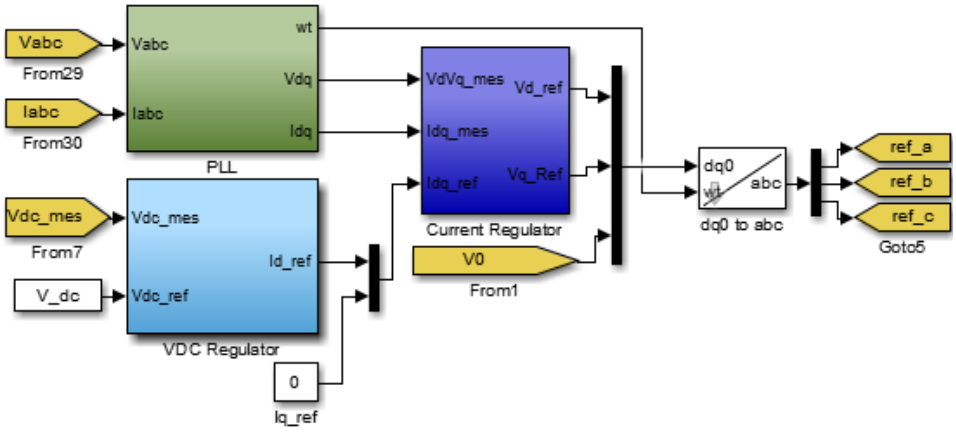

Figure C.1: Simulink diagram: Synchronous reference frame controller

Bibliography

[1] B. Xiao, L. Hang, J. Mei, C. Riley, L. Tolbert, and B. Ozpineci, "Modular cascaded h-bridge multilevel pv inverter with distributed mppt for grid-connected applications," *Industry Applications, IEEE Transactions on*, vol. 51, no. 2, pp. 1722–1731, March 2015.

[2] L. Liu, H. Li, Y. Xue, and W. Liu, "Decoupled active and reactive power control for large-scale grid-connected photovoltaic systems using cascaded modular multilevel converters," *Power Electronics, IEEE Transactions on*, vol. 30, no. 1, pp. 176–187, Jan 2015.

[3] J. Chavarria, D. Biel, F. Guinjoan, C. Meza, and J. Negroni, "Energy-balance control of pv cascaded multilevel grid-connected inverters under level-shifted and phase-shifted pwms," *Industrial Electronics, IEEE Transactions on*, vol. 60, no. 1, pp. 98–111, Jan 2013.

[4] B. Alajmi, K. Ahmed, G. Adam, S. Finney, and B. Williams, "Modular multilevel inverter with maximum power point tracking for grid connected photovoltaic application," in *Industrial Electronics (ISIE), 2011 IEEE International Symposium on*, June 2011, pp. 2057–2062.

[5] F. Schimpf, L. E. Norum *et al.*, "Grid connected converters for photovoltaic, state of the art, ideas for improvement of transformerless inverters," in *Nordic Workshop on Power and Industrial Electronics (NORPIE/2008), June 9-11, 2008, Espoo, Finland*. Helsinki University of Technology, 2008.

[6] S. Debnath, J. Qin, B. Bahrani, M. Saeedifard, and P. Barbosa, "Operation, control, and applications of the modular multilevel converter: A review," *Power Electronics, IEEE Transactions on*, vol. 30, no. 1, pp. 37–53, Jan 2015.

[7] A. Lesnicar and R. Marquardt, "An innovative modular multilevel converter topology suitable for a wide power range," in *Power Tech Conference Proceedings, 2003 IEEE Bologna*, vol. 3, June 2003, pp. 6 pp. Vol.3–.

[8] L. Harnefors, A. Antonopoulos, S. Norrga, L. Angquist, and H.-P. Nee, "Dynamic analysis of modular multilevel converters," *Industrial Electronics, IEEE Transactions on*, vol. 60, no. 7, pp. 2526–2537, July 2013.

[9] J. Qin and M. Saeedifard, "Predictive control of a modular multilevel converter for a back-to-back hvdc system," *Power Delivery, IEEE Transactions on*, vol. 27, no. 3, pp. 1538–1547, July 2012.

[10] H. Nademi, A. Das, and L. Norum, "Modular multilevel converter with an adaptive observer of capacitor voltages," *Power Electronics, IEEE Transactions on*, vol. 30, no. 1, pp. 235–248, Jan 2015.

[11] M. Perez, S. Bernet, J. Rodriguez, S. Kouro, and R. Lizana, "Circuit topologies, modeling, control schemes, and applications of modular multilevel converters," *Power Electronics, IEEE Transactions on*, vol. 30, no. 1, pp. 4–17, Jan 2015.

[12] W. Li, L.-A. Gregoire, and J. Bélanger, "Control and performance of a modular multilevel converter system," in *CIGRÉ Canada, Conference on Power Systems, Halifax*, 2011.

[13] A. Das, H. Nademi, and L. Norum, "A pulse width modulation technique for reducing switching frequency for modular multilevel converter," in *Power Electronics (IICPE), 2010 India International Conference on*, Jan 2011, pp. 1–6.

[14] S. Rohner, S. Bernet, M. Hiller, and R. Sommer, "Modulation, losses, and semiconductor requirements of modular multilevel converters," *Industrial Electronics, IEEE Transactions on*, vol. 57, no. 8, pp. 2633–2642, Aug 2010.

[15] K. Ilves, S. Norrga, L. Harnefors, and H.-P. Nee, "Analysis of arm current harmonics in modular multilevel converters with main-circuit filters," in *Systems, Signals and Devices (SSD), 2012 9th International Multi-Conference on*, March 2012, pp. 1–6.

[16] H. Nademi, "Advanced Control of Power Converters: Modular Multilevel Converter," Ph.D. dissertation, Norwegian University of Science and Technology, 2014.

[17] L. He, K. Zhang, J. Xiong, and S. Fan, "A repetitive control scheme for harmonic suppression of circulating current in modular multilevel converters," *Power Electronics, IEEE Transactions on*, vol. 30, no. 1, pp. 471–481, Jan 2015.

[18] Y. Deng, K. H. Teo, C. Duan, T. Habetler, and R. Harley, "A fast and generalized space vector modulation scheme for multilevel inverters," *Power Electronics, IEEE Transactions on*, vol. 29, no. 10, pp. 5204–5217, Oct 2014.

[19] J. Benner and L. Kazmerski, "Photovoltaics gaining greater visibility," *Spectrum, IEEE*, vol. 36, no. 9, pp. 34–42, Sep 1999.

[20] M. Villalva, J. Gazoli, and E. Filho, "Comprehensive approach to modeling and simulation of photovoltaic arrays," *Power Electronics, IEEE Transactions on*, vol. 24, no. 5, pp. 1198–1208, May 2009.

[21] C. Lashway, "Photovoltaic system testing techniques and results," *Energy Conversion, IEEE Transactions on*, vol. 3, no. 3, pp. 503–506, Sep 1988.

[22] A. Maki and S. Valkealahti, "Power losses in long string and parallel-connected short strings of series-connected silicon-based photovoltaic modules due to partial shading conditions," *Energy Conversion, IEEE Transactions on*, vol. 27, no. 1, pp. 173–183, March 2012.

[23] Y. Xue, K. Divya, G. Griepentrog, M. Liviu, S. Suresh, and M. Manjrekar, "Towards next generation photovoltaic inverters," in *Energy Conversion Congress and Exposition (ECCE), 2011 IEEE*, Sept 2011, pp. 2467–2474.

[24] H. Alatrash, R. Amarin, and C. Lam, "Enabling large-scale pv integration into the grid," in *Green Technologies Conference, 2012 IEEE*, April 2012, pp. 1–6.

[25] F. Blaabjerg, R. Teodorescu, M. Liserre, and A. Timbus, "Overview of control and grid synchronization for distributed power generation systems," *Industrial Electronics, IEEE Transactions on*, vol. 53, no. 5, pp. 1398–1409, Oct 2006.

[26] J. A. Houldsworth and D. A. Grant, "The use of harmonic distortion to increase the output voltage of a three-phase pwm inverter," *Industry Applications, IEEE Transactions on*, vol. IA-20, no. 5, pp. 1224–1228, Sept 1984.

[27] S.-K. Kim, J.-H. Jeon, C.-H. Cho, E.-S. Kim, and J.-B. Ahn, "Modeling and simulation of a grid-connected {PV} generation system for electromagnetic transient analysis," *Solar Energy*, vol. 83, no. 5, pp. 664 – 678, 2009. [Online]. Available: http://www.sciencedirect.com/science/article/pii/S0038092X08002843

[28] A. Jain and A. Kapoor, "A new method to determine the diode ideality factor of real solar cell using lambert w-function," *Solar Energy Materials and Solar Cells*, vol. 85, no. 3, pp. 391 – 396, 2005. [Online]. Available: http://www.sciencedirect.com/science/article/pii/S0927024804002442

[29] B. Subudhi and R. Pradhan, "A comparative study on maximum power point tracking techniques for photovoltaic power systems," *Sustainable Energy, IEEE Transactions on*, vol. 4, no. 1, pp. 89–98, Jan 2013.

[30] X. Liu and L. Lopes, "An improved perturbation and observation maximum power point tracking algorithm for pv arrays," in *Power Electronics Specialists Conference, 2004. PESC 04. 2004 IEEE 35th Annual*, vol. 3, June 2004, pp. 2005–2010 Vol.3.

[31] D. Sera, L. Mathe, T. Kerekes, S. Spataru, and R. Teodorescu, "On the perturb-and-observe and incremental conductance mppt methods for pv systems," *Photovoltaics, IEEE Journal of*, vol. 3, no. 3, pp. 1070–1078, July 2013.

[32] N. Femia, G. Petrone, G. Spagnuolo, and M. Vitelli, "Optimization of perturb and observe maximum power point tracking method," *Power Electronics, IEEE Transactions on*, vol. 20, no. 4, pp. 963–973, July 2005.

[33] J. Rawlings and D. Mayne, *Model Predictive Control: Theory and Design*. Nob Hill Pub., 2009. [Online]. Available: http://books.google.co.uk/books?id=3_rfQQAACAAJ

[34] B. Riar, T. Geyer, and U. Madawala, "Model predictive direct current control of modular multilevel converters: Modeling, analysis, and experimental evaluation," *Power Electronics, IEEE Transactions on*, vol. 30, no. 1, pp. 431–439, Jan 2015.

[35] J. Bocker, B. Freudenberg, A. The, and S. Dieckerhoff, "Experimental comparison of model predictive control and cascaded control of the modular multilevel converter," *Power Electronics, IEEE Transactions on*, vol. 30, no. 1, pp. 422–430, Jan 2015.

[36] J.-W. Moon, J.-S. Gwon, J.-W. Park, D.-W. Kang, and J.-M. Kim, "Model predictive control with a reduced number of considered states in a modular multilevel converter for hvdc system," *Power Delivery, IEEE Transactions on*, vol. PP, no. 99, pp. 1–1, 2014.

[37] S. Rivera, B. Wu, R. Lizana, S. Kouro, M. Perez, and J. Rodriguez, "Modular multilevel converter for large-scale multistring photovoltaic energy conversion system," in *Energy Conversion Congress and Exposition (ECCE), 2013 IEEE*, Sept 2013, pp. 1941–1946.